

# Polycomb Repressive Complex 2 and KRYPTONITE regulate pathogen-induced programmed cell death in *Arabidopsis*

Eva Dvořák Tomaščíková <sup>1,†</sup>, Anders Hafrén <sup>1</sup>, Minerva S. Trejo-Arellano <sup>1,†</sup>,  
Sheena Ricafranca Rasmussen <sup>1</sup>, Hikaru Sato <sup>1</sup>, Juan Santos-González <sup>1</sup>, Claudia Köhler <sup>1,§</sup>,  
Lars Hennig <sup>1</sup> and Daniel Hofius <sup>1,\*</sup>

<sup>1</sup> Department of Plant Biology, Uppsala BioCenter, Swedish University of Agricultural Sciences and Linnean Center for Plant Biology, SE-75007 Uppsala, Sweden

\*Author for communication: daniel.hofius@slu.se

<sup>†</sup>Present address: Institute of Experimental Botany, Czech Academy of Sciences; Centre of the Region Haná for Biotechnological and Agricultural Research, Šlechtitelů 31, 779 00 Olomouc, Czech Republic.

<sup>‡</sup>Present address: Department of Cell and Developmental Biology, John Innes Centre, Norwich NR4 7UH, UK

<sup>§</sup>Senior authors.

L.H., C.K., and D.H. designed the research. E.D.T., A.H., M.S.T.-A., S.R.R., H.S., and J.S.-G. performed experiments. E.D.T., A.H., M.S.T.-A., S.R.R., H.S., J.S.-G., C.K., and D.H. analyzed the data. C.K., D.H., and E.D.T., wrote the manuscript with contributions from all authors. All authors approved the final version of this manuscript.

The authors responsible for the distribution of the materials integral to the findings presented in this article in accordance with the policy described in the Instructions for Authors (<https://academic.oup.com/plphys/pages/general-instructions>) are: Daniel Hofius (daniel.hofius@slu.se), Claudia Köhler (claudia.kohler@slu.se)

## Abstract

The Polycomb Repressive Complex 2 (PRC2) is well-known for its role in controlling developmental transitions by suppressing the premature expression of key developmental regulators. Previous work revealed that PRC2 also controls the onset of senescence, a form of developmental programmed cell death (PCD) in plants. Whether the induction of PCD in response to stress is similarly suppressed by the PRC2 remained largely unknown. In this study, we explored whether PCD triggered in response to immunity- and disease-promoting pathogen effectors is associated with changes in the distribution of the PRC2-mediated histone H3 lysine 27 trimethylation (H3K27me3) modification in *Arabidopsis thaliana*. We furthermore tested the distribution of the heterochromatic histone mark H3K9me2, which is established, to a large extent, by the H3K9 methyltransferase KRYPTONITE, and occupies chromatin regions generally not targeted by PRC2. We report that effector-induced PCD caused major changes in the distribution of both repressive epigenetic modifications and that both modifications have a regulatory role and impact on the onset of PCD during pathogen infection. Our work highlights that the transition to pathogen-induced PCD is epigenetically controlled, revealing striking similarities to developmental PCD.

## Introduction

Cell-specific transcriptional programs are enabled by chromatin modifications that control the access of

transcriptional regulators during the appropriate stages of development (Bell et al., 2011). Polycomb group (PcG) proteins are major epigenetic controllers of cell identity that act by modifying histone tails and establish transcriptionally

repressive domains that are heritable over mitotic cell divisions (Yu et al., 2019). PcG proteins assemble into multimeric complexes that have histone-tail modifying enzymatic activities. In vegetative tissues of *Arabidopsis* (*Arabidopsis thaliana*), the Polycomb Repressive Complex 2 (PRC2) is composed of the partially redundant SET-domain proteins CURLY LEAF (CLF) and SWINGER (SWN), the WD-40 domain proteins FERTILIZATION INDEPENDENT ENDOSPERM and MULTICOPY SUPPRESSOR OF IRA 1, and the partially redundant zinc-finger proteins EMBRYONIC FLOWER 2 and VERNALIZATION 2. PRC2 complexes trimethylate histone H3 on lysine 27 (H3K27me<sub>3</sub>), a modification generally associated with transcriptional repression. Plant PRC2 controls major developmental transitions, like the transition to flowering, embryo to seedling transition, and endosperm initiation (Mozgova and Hennig 2015).

Senescence typically leads to the controlled death of individual cells, tissues, and organs, and can thus be considered a developmental form of programmed cell death (PCD; Thomas, 2013; Huysmans et al., 2017). Senescence is associated with genome-wide transcriptional reprogramming (Breeze et al., 2011; Guo and Gan, 2012) and can be prematurely triggered by the phytohormones abscisic acid (ABA) and ethylene as well as various environmental stresses (Iqbal et al., 2017; Yolcu et al., 2018), indicating that in the absence of inducing factors the onset of senescence is tightly suppressed. Loss of PRC2 function promotes ABA-induced senescence, revealing a role of the PRC2 in attenuating senescence initiation (Liu et al., 2019). Furthermore, the H3K27me<sub>3</sub> demethylase RELATIVE OF EARLY FLOWERING 6 (REF6) promotes leaf senescence by directly upregulating the expression of key regulators in this process (Wang et al., 2019), suggesting specific recruitment of REF6 upon senescence-promoting stimuli. In addition to changes in PRC2-mediated H3K27me<sub>3</sub>, senescence was previously shown to cause decondensation of chromocenters (Ay et al., 2014). Chromocenters are heavily marked by the heterochromatic H3K9me<sub>2</sub> histone modification that in *A. thaliana* is established by the SET-domain protein KRYPTONITE (KYP) and the partially redundantly acting proteins SUVH5 and SUVH6 (Jackson et al., 2002; Ebbs and Bender, 2006). Nevertheless, it remains to be shown whether chromocenter decondensation occurs during different forms of PCD and is accompanied by a redistribution of H3K9me<sub>2</sub>.

Pathogen invasion of plants is often associated with the rapid induction of PCD, either as part of immunity or disease (Dickman and Fluhr, 2013). The hypersensitive response (HR) is a localized PCD reaction that is activated by immune receptors upon recognition of pathogen-derived effector proteins, thereby confining the growth of (hemi)biotrophic microbes to the initial infection site (Coll et al., 2011; Mukhtar et al., 2016). In contrast, necrotrophic pathogens trigger host cell death by toxins and necrosis-inducing effectors to facilitate retrieval of nutrients from dead tissue for plant colonization (Lai and Mengiste, 2013). The transcriptional reprogramming during pathogen-induced PCD is

strikingly different from changes observed during different types of developmentally controlled PCD (Olvera-Carrillo et al., 2015), with the transcriptional signature of pathogen-triggered PCD being apparently defined by genes involved in defense rather than in a specific type of PCD (Huysmans et al., 2017). Recent studies revealed that epigenetic changes associate with defense responses (Zhou et al., 2010; Hwang et al., 2011; Downen et al., 2012; Le Roux et al., 2014; López Sánchez et al., 2016; Dutta et al., 2017); nevertheless, it remains unknown whether the activation of pathogen-induced PCD is associated with specific epigenetic signatures and is controlled by PRC2, similar to developmental PCD (Xu et al., 2016; Liu et al., 2019).

In this study, we explored whether PCD triggered in response to immunity- and disease-promoting pathogen effectors is associated with changes in PRC2-mediated H3K27me<sub>3</sub> and heterochromatic H3K9me<sub>2</sub> distribution. We furthermore tested whether the histone methyltransferase subunits from the PRC2 as well as KYP have a regulatory impact on pathogen-induced PCD. We report that effector-induced PCD causes major changes in the distribution of both repressive epigenetic modifications and that both modifications have a regulatory role on the onset of PCD. Our work highlights that the transition to pathogen-induced PCD is indeed epigenetically controlled, revealing striking similarities to developmentally-induced PCD.

## Results

### Inducible expression of AvrRpt2 and NPP1 triggers PCD

To investigate whether PRC2-mediated epigenetic changes associate with pathogen-induced PCD in *Arabidopsis*, we utilized the estradiol-inducible XVE system (Zuo et al., 2000) for the expression of two well-characterized effector proteins that were previously shown to trigger distinct PCD reactions in the absence of pathogen infection (Figure 1A; McNellis et al., 1998; Qutob et al., 2006; Elmore et al., 2012). The type III effector AvrRpt2 from the bacterium *Pseudomonas syringae* pv. *tomato* (*Pst*) strain DC3000 is recognized by the host immune receptor RESISTANCE TO *P. SYRINGAE* 2 (RPS2), resulting in the activation of immunity-related HR (Mackey et al., 2003; Lim and Kunkel, 2004). Necrosis-inducing *Phytophthora* protein 1 (NPP1; Fellbrich et al., 2002) from the oomycete *Phytophthora parasitica* (also termed NLP<sub>Pp</sub>; Qutob et al., 2006) is a pore-forming cytotoxin, which binds to a sphingolipid receptor on the extracellular side of the plasma membrane (Lenarčič et al., 2017). The membrane-disrupting activity of NPP1 triggers disease-related necrotic cell death, which differs genetically from the HR (Qutob et al., 2006). To facilitate NPP1 targeting to the apoplast, the effector was cloned in translational fusion with a plant signal peptide (SP; Rauhut et al., 2009; Figure 1A). We verified in selected transgenic lines that estradiol-induced accumulation of both effector proteins (Figure 1B) resulted in the induction of PCD, as monitored by increased electrolyte leakage and the development of cell death symptoms in comparison to the

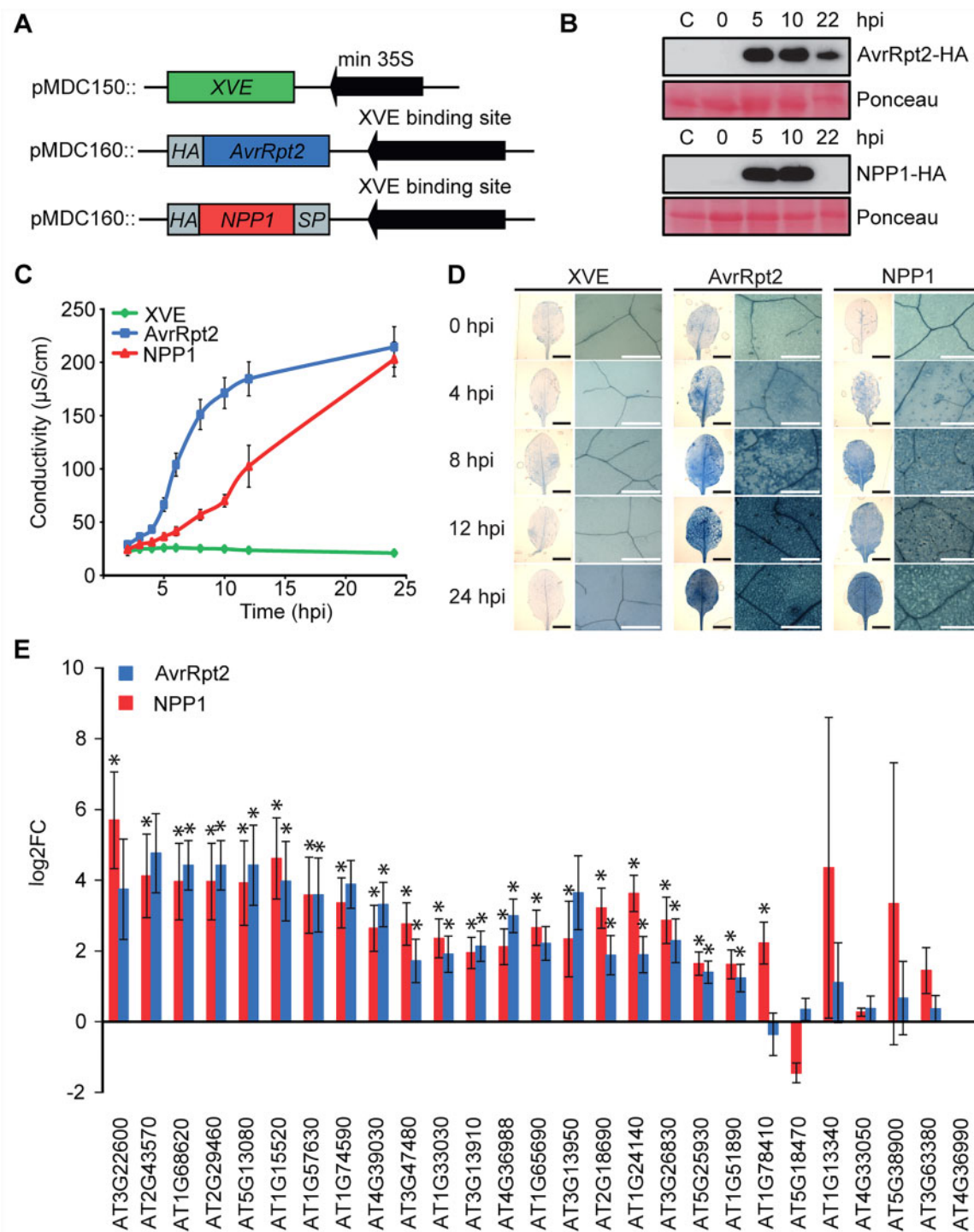


**Figure 1** Reliability of the two-component vector system for induction of effector-mediated PCD. A, Schematic representation of the different constructs that were used for PCD induction. The activator vector, pMDC150::XVE, contains the chimeric transcription factor XVE under control of the minimal 35S promoter, while the pMDC160 responder vector contains the XVE-responsive promoter driving expression of *NPP1* and *AvrRpt2* upon XVE binding. *NPP1* is cloned in translational fusion with a SP for apoplastic delivery, and both effector constructs contain a 3 × HA epitope tag. B, Immunoblot analysis of *AvrRpt2* (upper panel) and *NPP1* (lower panel) protein levels in transgenic *A. thaliana* at the indicated time points after  $\beta$ -estradiol induction, using an anti-HA antibody. Ponceau staining verified comparable protein loading. hpi, hours post induction. C, Electrolyte leakage from leaf discs of transgenic lines at 1–24 h after estradiol-induced *AvrRpt2* and *NPP1* expression in comparison to the XVE vector control. Mean and standard deviation (SD) were calculated from four disks per treatment with four replicates within an experiment. D, Trypan blue staining of dead cells in 6-week-old rosette leaves at the indicated time points after estradiol-induced effector accumulation. Scale bars represent 1 mm (whole leaves) or 100  $\mu\text{m}$ . (E) Biotic stress-induced PCD markers (Olvera-Carrillo et al., 2015) were significantly upregulated at 12 h after induction of *NPP1*- and *AvrRpt2*-mediated PCD as detected by RNAseq. Asterisks indicate  $\text{FDR} \leq 0.05$ .

transactivator XVE alone (Figure 1C and D; Supplemental Figure S1A and B). Expression of AvrRpt2 caused faster induction and higher levels of electrolyte leakage compared to NPP1 (Figure 1C), which agreed with the earlier and more severe appearance of trypan blue-stained dead cells (Figure 1D) and macroscopic tissue collapse (Supplemental Figure S1B) in AvrRpt2 expressing plants.

To investigate the transcriptional response upon PCD induction, we performed RNA sequencing (RNAseq) of leaf tissue 12 h after induction of the respective effectors (Supplemental Data Set S1A). This time point was selected as both AvrRpt2 and NPP1 expressing leaves showed a significant increase in ion leakage indicative of PCD activation, yet without a vast tissue collapse that could bias the analyses (Figure 1C; Supplemental Figure S1B). Initial inspection of the transcriptomes revealed that out of 27 previously identified “biotic marker genes” of PCD (Olvera-Carrillo et al., 2015), 20 were strongly upregulated after both AvrRpt2 and NPP1 induction (Figure 1E). Collectively, these data show that expression of AvrRpt2 and NPP1 reliably induces PCD, supporting the suitability of this system to study epigenetic changes associated with PCD.

### The *A. thaliana* transcriptome is quickly reshaped upon PCD induction

A principal component analysis of all transcriptomes revealed that expression of AvrRpt2 and NPP1 caused a transcriptome response that clearly differed from the XVE empty vector (Supplemental Figure S2A). We obtained 11,700 differentially expressed genes (DEGs) associated with AvrRpt2 and 9,900 DEGs associated with NPP1 expression. Additionally, we detected 519 and 464 differentially expressed transposable elements (TEs) after AvrRpt2 and NPP1 induction, respectively ( $P < 0.05$ ,  $\log_2FC \geq 1$  for upregulated genes,  $\log_2FC \leq -1$  for downregulated genes; Figure 2A and B; Supplemental Data Sets S2 and S3). We validated RNAseq data by reverse transcription-quantitative PCR (RT-qPCR) for randomly selected top-misregulated genes specific for AvrRpt2 and NPP1 expression and found that the transcriptome data were in good agreement with the RT-qPCR data (Supplemental Figure S2B). Furthermore, comparison with previously published *A. thaliana* transcriptomes at 12 h after infection with avirulent strain *Pst* DC3000 AvrRps4 (Howard et al., 2013) and at 4 h after NLP<sub>pp</sub> infection (Qutob et al., 2006), revealed a significant overlap between the DEGs identified in our system and the previously published datasets (Supplemental Figure S2C and D).

We compared DEGs induced by AvrRpt2 and NPP1 expression and found a strong overlap for up- as well as downregulated DEGs ( $P < 0.001$ , hypergeometric test; Figure 2A). Commonly downregulated genes were enriched for gene ontologies (GOs) related to photosynthesis, transcription, metabolic processes, growth-related processes, and DNA methylation (Figure 2C). Commonly upregulated genes were enriched for GOs related to immunity- and cell death-

related processes (Figure 2D). There were only a few significantly enriched GOs specific for either AvrRpt2- or NPP1-induced PCD. Among those, fatty acid catabolism and hydrogen peroxide (H<sub>2</sub>O<sub>2</sub>) response were specifically enriched GOs for AvrRpt2-induced upregulated genes, consistent with a well-established role for fatty acid and H<sub>2</sub>O<sub>2</sub> signaling in HR execution and systemic acquired resistance activation (Montillet et al., 2005; Zoeller et al., 2012; Lim et al., 2017). The NPP1-specific enrichment of upregulated genes related to immune system processes reflects the unique immunogenic activities of cytotoxic NLP proteins (Böhm et al., 2014; Albert et al., 2015), whereas enrichment of genes related to SP processing and vesicle-mediated transport are likely caused by the activation of secretion-dependent defenses upon recognition of NPP1 in the apoplast.

### Effector-induced PCD is associated with a decrease in nuclei size, chromocenter relaxation, and H3K9me2 redistribution

*Arabidopsis thaliana* leaf mesophyll interphase nuclei typically have 6–10 discrete, intensely DAPI-stained “heterochromatic” domains known as chromocenters (Fransz et al., 2002). Previous work revealed that leaf senescence was associated with decondensation of chromocenters (Ay et al., 2014). We therefore investigated whether effector-induced PCD caused a similar effect on the level of chromocenter condensation. Indeed, we observed a significant decrease in the number of chromocenters in PCD-induced AvrRpt2 and NPP1 samples that were connected with a decrease in nuclear size (Figure 3A and B). Decondensation of chromocenters during effector-induced PCD was corroborated by analyzing the distribution of centromeric 180 bp repeat DNA sequences using fluorescence in situ hybridization (FISH). We divided the observed signals into four categories based on the nuclear area (normal, small) and the compactness of the signal (condensed, decondensed): Class I: normal-sized nuclei, condensed; Class II: normal-sized nuclei, decondensed; Class III: small nuclei, condensed, and class IV: small nuclei, decondensed (Figure 3C). While in the control most of the nuclei had compact 180 bp centromeric repeat sequences (Class I, ~80%), NPP1, and more prominently AvrRpt2 nuclei contained small nuclei with decondensed centromeric repeat sequences (Class IV, 10% and 50%, respectively; Figure 3D), supporting the notion that chromocenters become highly decondensed during PCD. Chromocenter decondensation during senescence is not connected with a global loss of the heterochromatic mark H3K9me2; instead, this modification becomes more widely distributed, possibly invading non-heterochromatic regions (Ay et al., 2014). We tested whether decondensation of chromocenters would cause a similar redistribution of H3K9me2 by profiling this mark using chromatin immunoprecipitation followed by sequencing (ChIPseq) in XVE, AvrRpt2, and NPP1 samples (Supplemental Data Set S1B; Supplemental Figures S3 and S4). We found substantially more TEs losing H3K9me2 in AvrRpt2 than in NPP1

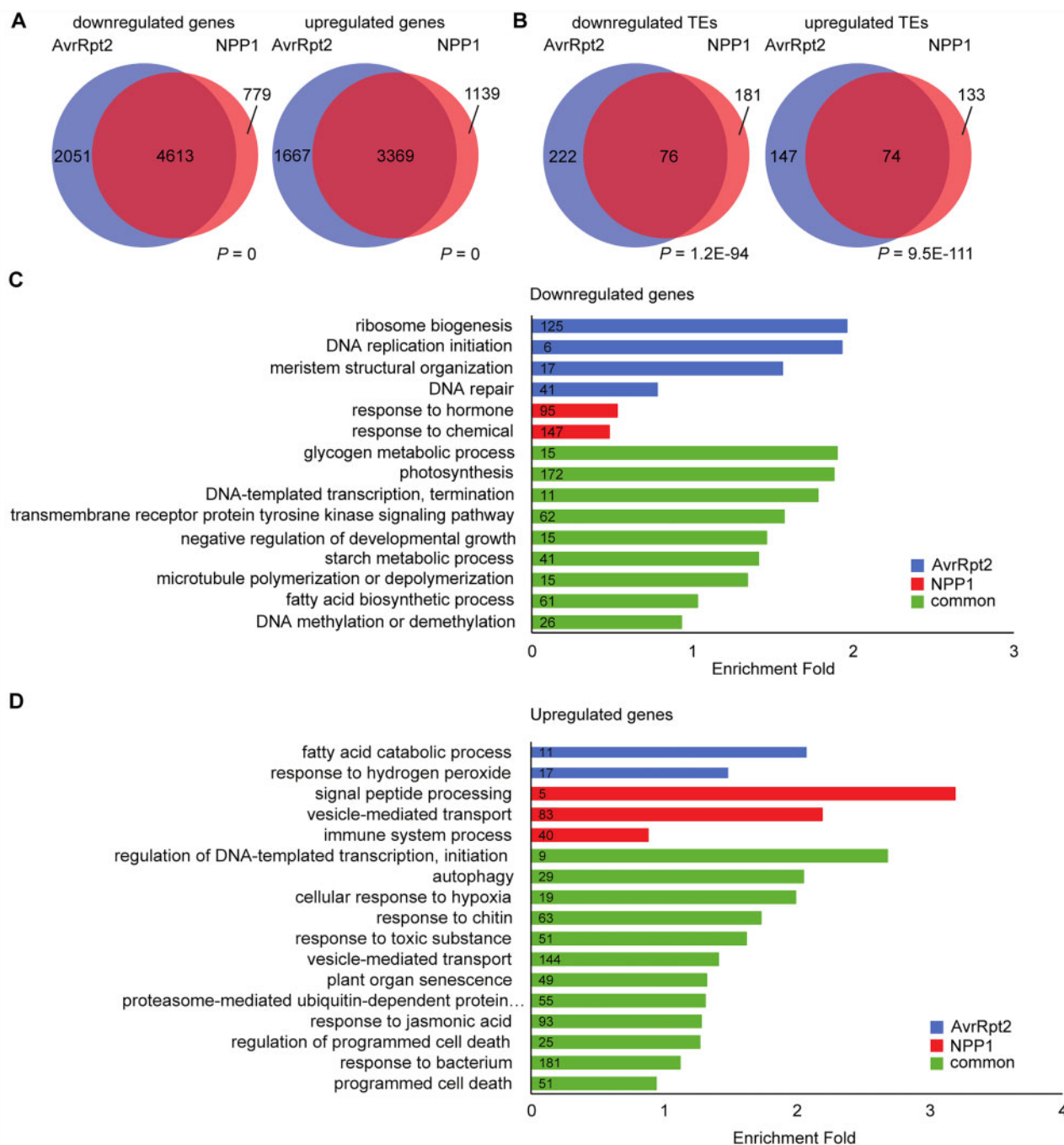


**Figure 2** Overlapping transcriptional changes 12 h after AvrRpt2- and NPP1-mediated induction of PCD. A and B, Venn diagrams showing overlap of differentially upregulated and downregulated genes (A) and TEs (B) during two types of PCD. Statistical significance was calculated using a hypergeometric test. C and D, GO term analyses of specific and common downregulated (C) and upregulated (D) genes.  $P < 0.001$  according to PLAZA version 4.0. Numbers within bars correspond to gene numbers in respective GO category.

samples. The majority of TEs losing H3K9me2 in NPP1 overlapped with those losing H3K9me2 in AvrRpt2 (Figure 4B). Those TEs that specifically lost H3K9me2 in AvrRpt2 and NPP1 were depleted for gypsy TEs (Figure 4C, Supplemental Figure 5SA). There were more TEs gaining H3K9me2 in NPP1 samples compared to AvrRpt2. Additionally, there was a significant proportion of TEs gaining H3K9me2 being common for AvrRpt2 and NPP1 samples (Figure 4B). TEs gaining

H3K9me2 specifically in NPP1 were enriched for gypsy TEs (Figure 4D; Supplemental Figure 5SB), revealing that the epigenetic status of this class of TEs is specifically sensitive during PCD induction. We also identified about 800 genes losing and 500 genes gaining H3K9me2 in AvrRpt2 and NPP1 samples, with most of them being shared between both treatments (Figure 4A). Gain of H3K9me2 was negatively associated with gene expression, while loss of H3K9me2 did

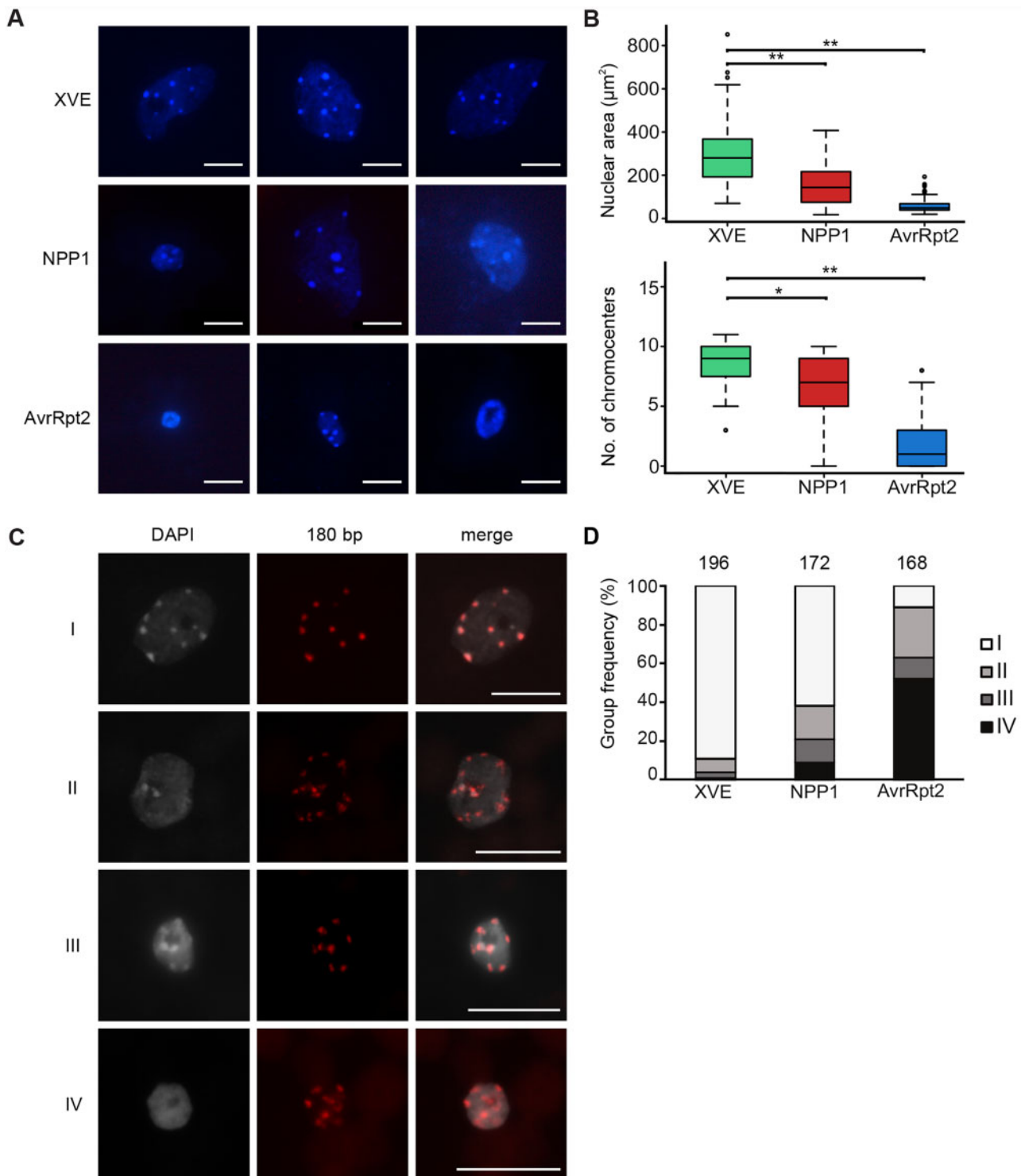


**Figure 3** Chromatin organization of interphase nuclei 12 h after induction of PCD. A, Representative DAPI-stained nuclei from the 5th leaf of 6-week-old plants with  $\beta$ -estradiol-induced PCD. Bar =  $10\ \mu\text{m}$ . B, Boxplots representing the distribution of nuclear area (top) and the number of chromocenters (bottom),  $*P < 0.05$ ,  $**P < 0.01$  in a Wilcoxon statistical test. Nuclear area,  $n > 100$ ; number of chromocenters,  $n > 50$ . The lower and upper hinges of the boxplots correspond to the first and third quartiles of the data, the black lines within the boxes mark the median. Whiskers mark 10 and 90 percent intervals and all data points which lie beyond the extremes of the whiskers are outliers. C, Representative DNA-FISH of 180 bp centromeric repeats. Nuclei were classified in four classes based on size and chromatin condensation. Class I: normal-sized nuclei, condensed, Class II: normal-sized nuclei, decondensed, Class III: small nuclei, condensed, Class IV: small nuclei, decondensed. Bar =  $10\ \mu\text{m}$ . D, Proportion of nuclei belonging to respective classes. Numbers on top of bars correspond to total numbers of analyzed nuclei.

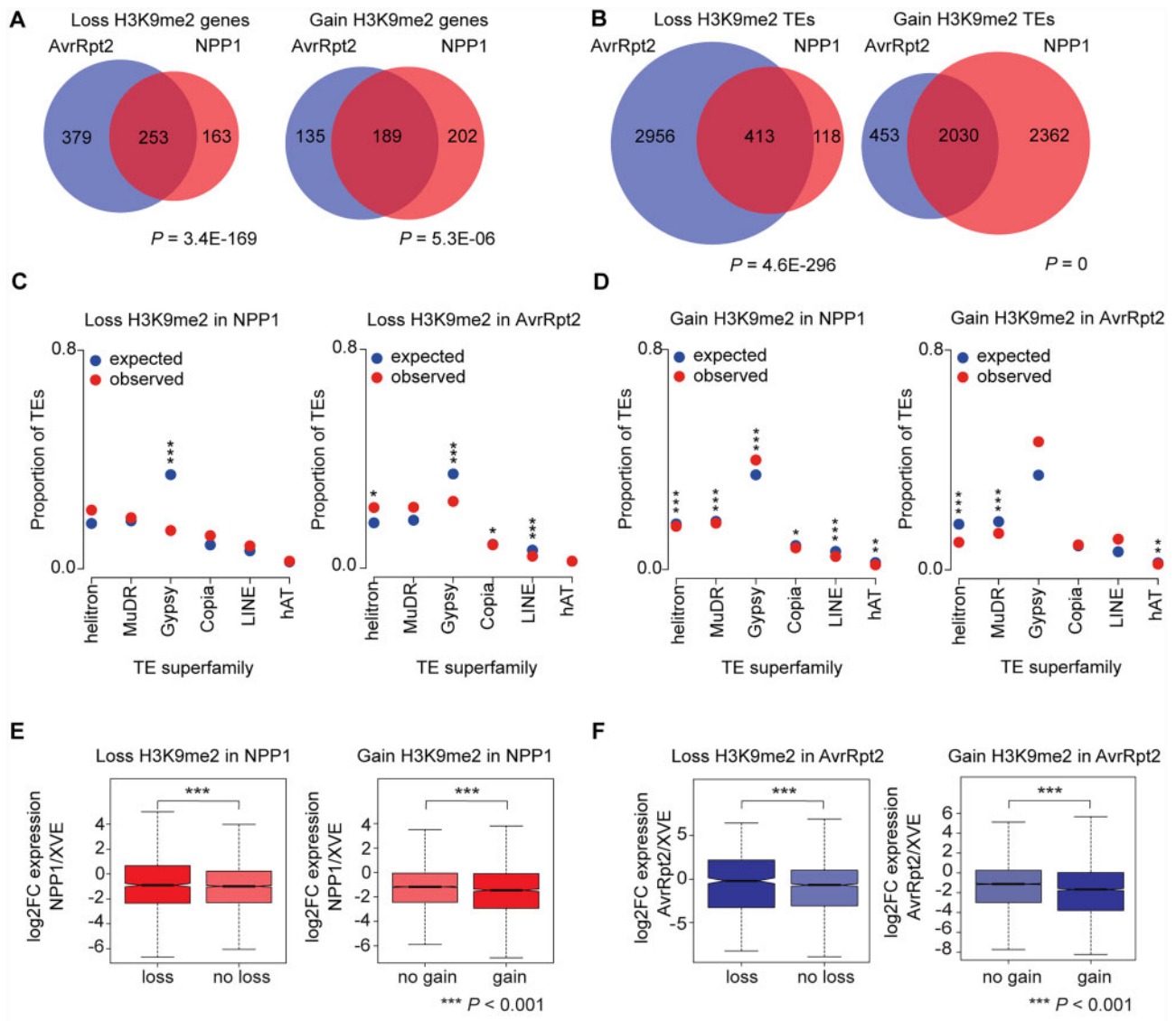


**Figure 4** Conserved and specific redistribution of the heterochromatic mark H3K9me2 during AvrRpt2- and NPP1-induced PCD. A and B, Venn diagrams showing overlap of genes (A) and TEs (B) gaining and losing H3K9me2 during two types of PCD. Statistical significance was calculated using a hypergeometric test. C and D, Proportion of specific TE families losing (C) and gaining (D) H3K9me2 upon NPP1 and AvrRpt2 expression. \*\*\* indicates  $P < 0.001$ , \*\* $P < 0.01$ , \* $P < 0.05$  based on chi-square testing. All annotated TEs from each class were tested. E and F, Boxplots showing expression changes of genes gaining or losing H3K9me2 upon NPP1 (E) and AvrRpt2 (F) expression. Genes were sorted into quartiles based on their loss or gain of H3K9me2. For genes losing H3K9me2, the first quartile was compared against the rest, and significance was tested by using a Kolmogorov–Smirnov test ( $***P < 0.001$ ). For genes gaining H3K9me2, the first three quartiles were compared against the fourth, and significance was tested by using a Kolmogorov–Smirnov test ( $***P < 0.001$ ). The lower and upper hinges of the boxplots correspond to the first and third quartiles of the data, the black lines within the boxes mark the median.

not cause gene activation (Figure 4E and F). However, among genes gaining H3K9me2, we did not identify significantly enriched gene categories, suggesting that H3K9me2 is not specifically targeted to new regions. Instead, H3K9me2 rather invades non-heterochromatic regions as previously proposed (Ay et al., 2014), having a negative impact on the expression of the genes located in the invaded regions. Together, we conclude that effector-induced PCD is associated with changes in H3K9me2 distribution, correlating with a strong decrease in nuclei size and chromocenter relaxation.

### Changes in gene expression correlate with loss of H3K27me3

The PRC2 regulates major transitions during plant development (Mozgova and Hennig, 2015). We, therefore, addressed the question whether the transition to PCD would be connected to changes in H3K27me3 distribution. We profiled H3K27me3 distribution by ChIPseq in triplicates upon PCD induction by AvrRpt2 and NPP1 expression (Supplemental Data Set S1B; Supplemental Figure S3). We identified 2,158 genes losing H3K27me3 in AvrRpt2 and NPP1 expressing

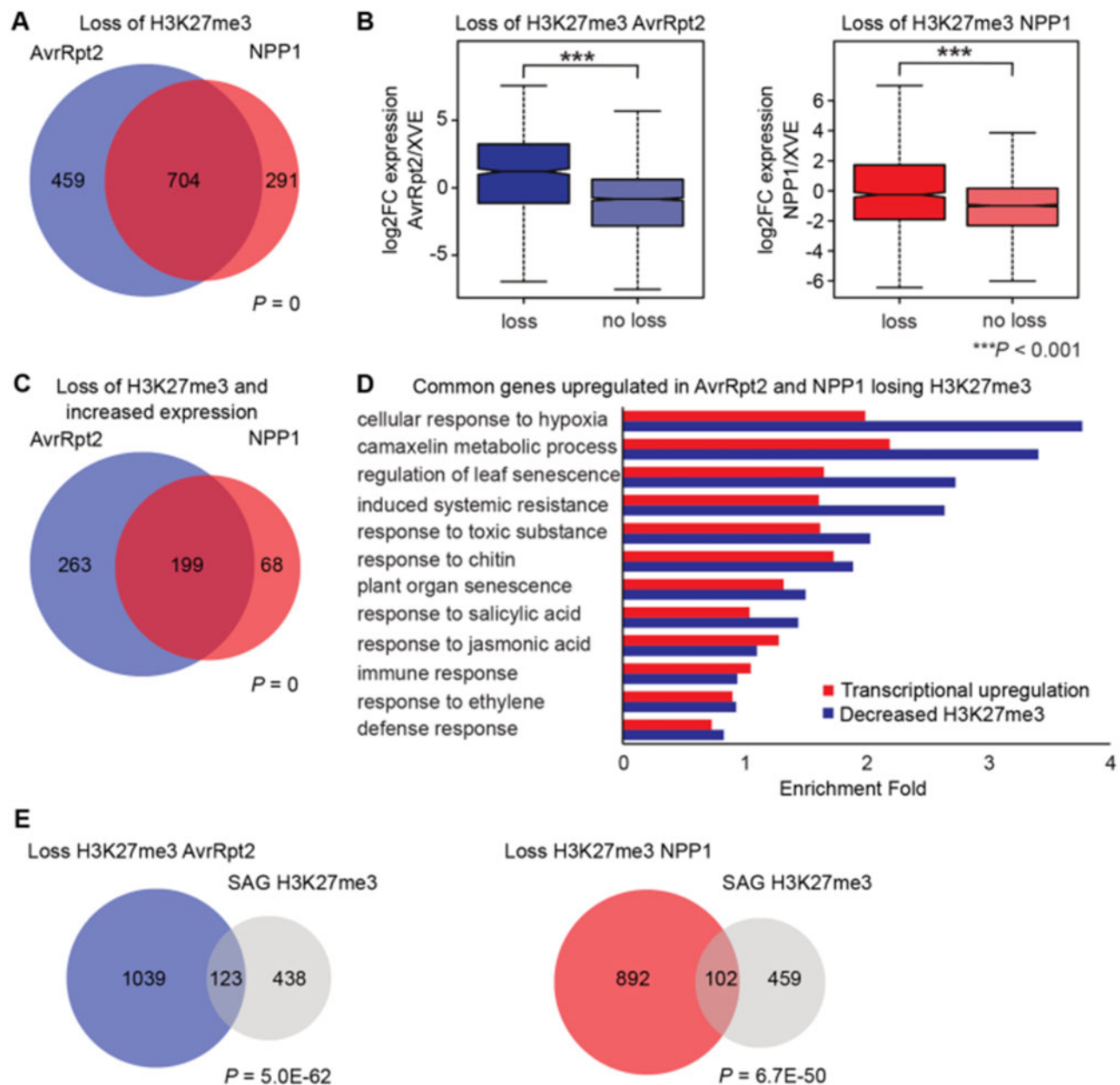


**Figure 5** Loss of H3K27me3 associates with increased expression of genes related to pathogen response and PCD. A, Venn diagram showing overlap of genes losing H3K27me3 in NPP1- and AvrRpt2-induced PCD. Statistical significance was calculated using a hypergeometric test. B, Boxplots showing expression of genes losing H3K27me3. Genes were sorted into quartiles. The first quartile was compared against the rest and significance was tested by using a Kolmogorov–Smirnov test ( $***P < 0.001$ ). The lower and upper hinges of the boxplots correspond to the first and third quartiles of the data, the black lines within the boxes mark the median. C, Venn diagram showing overlap of upregulated genes with reduced H3K27me3 upon AvrRpt2 and NPP1 induction. Statistical significance was calculated using a hypergeometric test. D, GO enrichment analyses of genes commonly losing H3K27me3 and being upregulated in AvrRpt2- and NPP1-induced PCD.  $P < 0.001$  according to PLAZA version 4.0. E, Genes losing H3K27me3 significantly overlapped with ABA-induced SAGs in both, AvrRpt2 (left Venn diagram) and NPP1 (right Venn diagram)-induced PCD. Significance was tested using a hypergeometric test.

samples, with 704 genes being commonly affected in both samples (Figure 5A; Supplemental Data Set S4). Genes losing H3K27me3 had increased expression, suggesting that changes in PRC2 targeting are functionally connected to PCD (Figure 5B). There was a significant overlap of genes that lost H3K27me3 and were significantly upregulated both in AvrRpt2 and NPP1 (Figure 5C; Supplemental Data Set

SSA). Those commonly deregulated genes were significantly enriched for functional categories related to defense responses as well as senescence, indicating that PRC2 may be involved in triggering the cellular reprogramming to PCD (Figure 5D).

Previous work revealed that ABA-induced senescence-associated genes (SAGs) are marked by H3K27me3; however,

only <2% (13) of those genes lose H3K27me3 upon ABA activation (Liu et al., 2019). Of the 561 H3K27me3-marked ABA-induced SAGs (Liu et al., 2019), >100 genes overlapped with genes losing H3K27me3 upon PCD induction (Figure 5E). Thus, ABA and pathogen effector treatment affect a common set of PRC2 targets, but effector-induced PCD affects more genes than ABA treatment.

The plant hormone ethylene plays a key role in the regulation of senescence and other forms of developmental PCD (Huysmans et al., 2017), but has also been implicated in the onset of HR-like cell death and activation of defense responses (Bouchez et al., 2007; Liu et al., 2008). We found a small, yet significant overlap of target genes of the ethylene signaling key regulator ETHYLENE INSENSITIVE3 (Chang et al., 2013) with genes losing H3K27me3 upon AvrRpt2- and NPP1-triggered PCD (Supplemental Figure S6A). Salicylic acid (SA) and jasmonic acid (JA) are also well-known hormones in the control of cell death, pathogen resistance, and senescence (Bari and Jones, 2009; Thaler et al., 2012; Kim et al., 2015; Radojčić et al., 2018). Similar to ethylene-regulated genes, genes induced by JA and SA (Hickman et al., 2017; Jin et al., 2018) significantly overlapped with genes losing H3K27me3 upon effector-triggered PCD (Supplemental Figure S6B and C), reflected in joint Gene Ontology (GO) categories like defense response and senescence (Supplemental Data Set S6). Together, these data support a regulatory role of several hormonal signaling pathways in pathogen-related cell death and imply similarities with the control of developmental PCD such as senescence.

### Genes gaining H3K27me3 upon effector-induced PCD are enriched for transcriptional regulators

Strikingly, we did not only identify genes losing H3K27me3, but many genes gained H3K27me3 during PCD induction. We identified 2,120 and 570 genes with increased H3K27me3 in AvrRpt2 and NPP1 expressing samples, respectively (Supplemental Data Set S4). More than half (365) of the genes gaining H3K27me3 in NPP1 samples overlapped with genes gaining H3K27me3 in AvrRpt2 samples (Figure 6A). The gain of H3K27me3 associated with reduced gene expression (Figure 6B; Supplemental Data Set S5B), indicating that PRC2 has an active role in cellular reprogramming during PCD. The vast majority of genes gaining H3K27me3 during effector-triggered PCD induction was previously identified as PRC2 targets in 3-week-old *Arabidopsis* leaves (Moreno-Romero et al., 2016; Figure 6C), revealing that those genes are not de novo PRC2 targets, but rather gain H3K27me3 during PCD (Figure 6D).

To understand the biological relevance of genes gaining H3K27me3 during effector-induced PCD, we identified GOs among downregulated genes upon AvrRpt2-induced PCD with or without gaining of H3K27me3. Downregulated genes not gaining H3K27me3 were enriched for GOs related to photosynthesis (Figure 6E), while downregulated genes gaining H3K27me3 were enriched for GOs as transcription

factors, plant development, and cell fate (Figure 6F). Among those transcription factors gaining H3K27me3, we found NAC and MAD5-box transcription factors as well as AT-hook-like gene families to be significantly enriched, with up to 30% of all genes from a particular family gaining H3K27me3 (Table 1). Previous studies revealed the importance of NAC transcription factors as positive and negative regulators of senescence (Podzimska-Sroka et al., 2015). Consistently, we observed gain of H3K27me3 in genes encoding NAC transcription factors NAC007/VND4, NAC009, NAC026/VND5, NAC030, NAC057, NAC070, and NAC105/VND3 that all were previously reported to be downregulated either during senescence or xylem vessel formation, another form of developmentally regulated PCD (Balazadeh et al., 2010; Breeze et al., 2011; Kim et al., 2018; Safavi-Rizi et al., 2018). VND4, VND5, and NAC057 were likewise downregulated in our transcriptome analyses upon effector-mediated PCD induction (Supplemental Figure S7).

We identified enriched hexamer motifs in the promoters of the top 200 downregulated genes with and without gaining of H3K27me3 upon AvrRpt2-induced PCD. The promoter regions of downregulated genes gaining H3K27me3 were enriched for TATA-related hexamers and an ABA-responsive element-related G-box core motif (Figure 6G), consistent with previous work showing that H3K27me3 buffers the activation of ABA-induced senescence-related genes (Liu et al., 2019). Gain of H3K27me3 may be necessary to prevent transcriptional activators from binding to the G-box motif. Consistent with the enrichment of photosynthesis-related GOs among H3K27me3-independent downregulated genes, the promoter regions of those genes were enriched for binding motifs of transcription factors related to light responses (Figure 6H), such as ABA INSENSITIVE 4 (core-binding motif, CCAC; Koussevitsky et al., 2007; Wang et al., 2018), PHYTOCHROME INTERACTING FACTOR 4 (CACATG; Zhang et al., 2013), and TCP4 (GGACCA; Dong et al., 2019). Previous studies revealed that GAGA-binding proteins function to recruit PRC2 complexes in *Arabidopsis* and *Drosophila* (Kassis and Brown, 2013; Hecker et al., 2015; Xiao et al., 2017). Interestingly, we found GAGA-related motifs to be enriched in the promoter regions of 109 downregulated genes that gained H3K27me3 and were bound by the PRC2 subunits CLF and SWN under normal conditions (Shu et al., 2019; Figure 6I; Supplemental Data Set S7). These data suggest that in addition to the GAGA motif, other motifs are used to recruit the PRC2 upon effector-induced PCD. Finally, we tested whether downregulated genes gaining H3K27me3 were deregulated in *clf swn* double mutants under normal conditions according to published transcriptome data (Shu et al., 2019; Supplemental Data Set S7). Among those effector-triggered downregulated PRC2 targets, we found many transcription factor genes related to plant development that were upregulated in *clf swn* double mutants, such as BUMBERSHOOT (Jasinski et al., 2005), AGAMOUS-LIKE 24 (AGL24; Liu et al., 2008), and NGATHAS (NGAs; Trigueros et al., 2009; Supplemental Data Set S7).

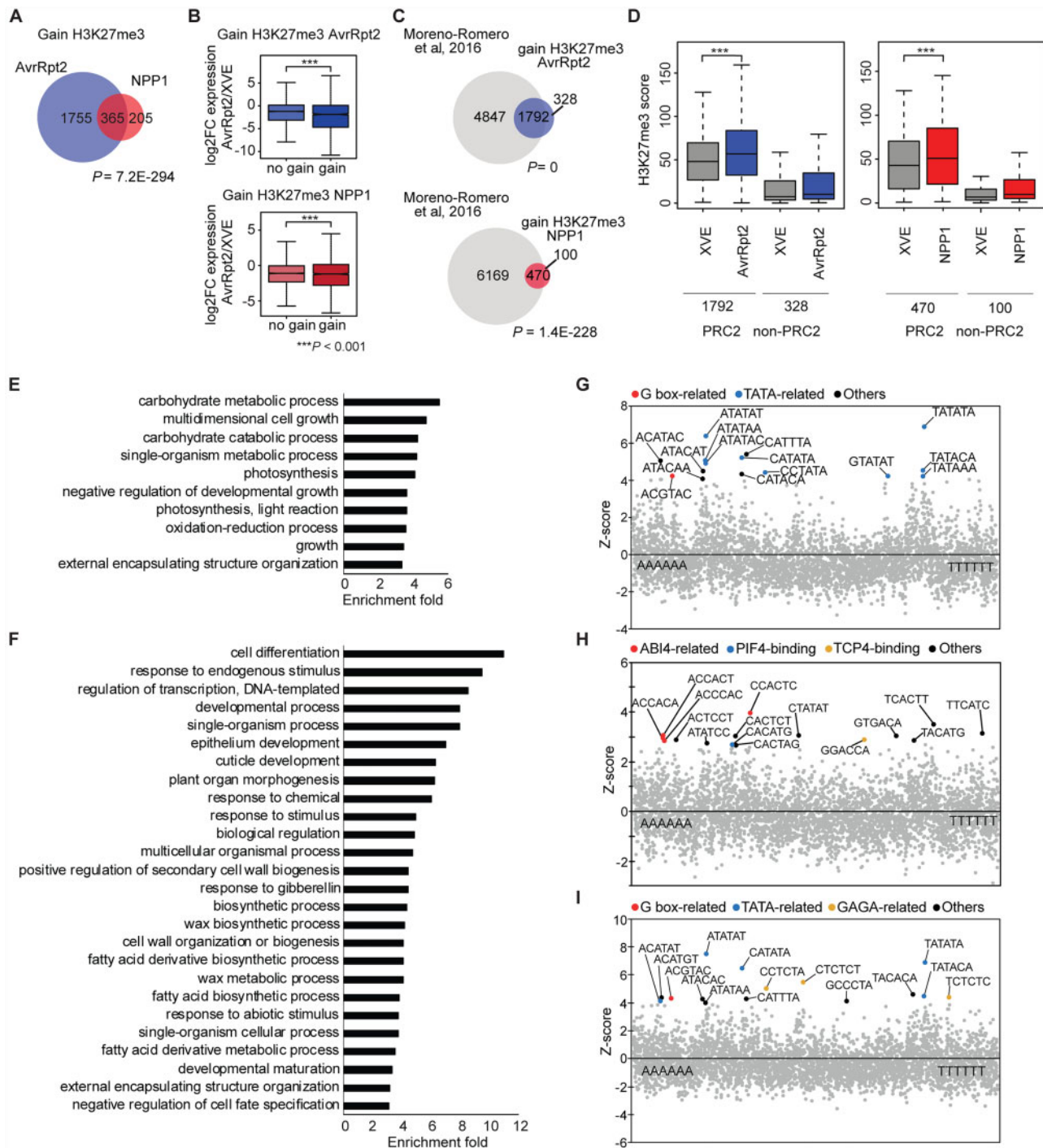


**Figure 6** Analysis of CLF/SWN PRC2-specific gene suppressive mechanisms upon effector-induced PCD. A, Venn diagram showing overlap of genes gaining H3K27me3 in NPP1- and AvrRpt2-induced PCD. Statistical significance was calculated using a hypergeometric test. B, Boxplots showing expression of genes gaining H3K27me3. Genes were sorted into quartiles. The first three quartiles were compared against the fourth and significance was tested by using a Kolmogorov–Smirnov test ( $***P < 0.001$ ). The lower and upper hinges of the boxplots correspond to the first and third quartiles of the data, the black lines within the boxes mark the median. C, Venn diagrams showing overlap of genes gaining H3K27me3 upon PCD induction with known PRC2 targets. Statistical significance was calculated using a hypergeometric test. D and E, Boxplots showing H3K27me3 scores of PRC2 target and non-target genes upon mock (XVE) and AvrRpt2 (D) and NPP1 (E) induction. Significance was tested by using a Wilcoxon statistical test ( $***P < 0.001$ ). F, GO analysis using downregulated genes gaining H3K27me3 upon AvrRpt2-induced PCD. The lower and upper hinges of the boxplots correspond to the first and third quartiles of the data, the black lines within the boxes mark the median. G–I, Overrepresentation analysis of hexamer motifs in the promoters of top 200 downregulated genes with (G) and without (H) gaining H3K27me3 upon AvrRpt2-induced PCD. (I) All 109 downregulated genes gaining H3K27me3 upon AvrRpt2-induced PCD that were bound by CLF or SWN. Z-scores (y-axis) for the observed frequencies of all hexamer motifs (x-axis) were presented in the scatter plot. The top 15 enriched motifs among each set of genes are highlighted in color. Genes bound by CLF or SWN were defined as those with H3K27me3 and binding of CLF or SWN based on previous work (Shu et al., 2019).

**Table 1** Transcription factors gaining H3K27me3 upon AvrRpt2-induced PCD

Transcription factor families	Total no. of genes in family	No. of genes in family gaining H3K27me3	Percent of total	P-value
NAC	96	31	32.3	4.0E-15
Agamous-like MADS box	108	34	31.5	5.7E-16
AT-hook motif nuclear localized	29	8	27.6	6.2E-05
MYB	131	30	22.9	2.4E-10
bHLH	162	24	14.8	4.9E-05
AP/EREBP	138	17	12.3	3.7E-03
WRKY	72	8	11.1	4.3E-02

The total number of transcription factors in each family, the number of genes in each family that is gaining H3K27me3, and their percentage of the total family members are indicated. Statistical significance was calculated using a hypergeometric test.

Among those transcription factors was NGATHA1 that was previously shown to induce ABA biosynthesis (Sato et al., 2018), suggesting that PRC2-induced repression of transcriptional regulators may dampen the effector-triggered PCD response.

### Epigenetic changes are functionally relevant for pathogen-triggered PCD

To investigate whether changes in H3K27me3 associated with pathogen-induced PCD are functionally relevant, we monitored HR development in knockout mutants of *CLF* and *SWN* upon infection with an AvrRpt2 expressing avirulent strain of *Pst* DC3000. The loss-of-function mutant of *NON-RACE-SPECIFIC DISEASE RESISTANCE 1* (*NDR1*), which is fully compromised in RPS2-mediated HR, served as a negative control for proper PCD induction (Munch et al., 2015; Schultz-Larsen et al., 2018). We found that loss of *SWN* caused a significantly increased electrolyte leakage during the time course of AvrRpt2-triggered HR compared to wild-type (Figure 7A), revealing the role of *SWN* in attenuating PCD. The knockout mutant of *CLF* did not show a significant effect, suggesting that *CLF* and *SWN* have partially non-redundant functions during the HR (Figure 7B). Intriguingly, we also observed consistently increased electrolyte leakage in the loss-of-function mutant of the major H3K9me2 methyltransferase *KYP* (Jackson et al., 2002) compared to wild-type (Figure 7C), indicating that changes in H3K9me2 distribution during PCD are functionally relevant.

To further investigate whether the observed effects also apply to HR triggered by a different bacterial effector, we assessed ion leakage during infection with an AvrRpm1 containing *Pst* DC3000 strain. AvrRpm1 is perceived by the immune receptor RESISTANCE TO *P. SYRINGAE* PV MACULICOLA 1 (*RPM1*) and induces an HR that engages multiple and partially different PCD pathways compared to those activated by RPS2 upon AvrRpt2 recognition (Hatsugai et al., 2009; Hofius et al., 2009; Coll et al., 2010). We observed significantly increased ion leakage during the initial phase of HR in both *swn* and *clf* mutants compared to wild-type (Figure 7D and E), whereas the *kyp* mutant maintained higher leakage levels throughout the HR (Figure 7F). These data corroborate the role of PRC2-mediated H3K27me3 in attenuating the onset of pathogen-

triggered HR as well as the importance of altered H3K9me2 distribution for PCD progression.

To finally analyze whether the differences in HR cell death resulted in altered disease resistance of the epigenetic mutants, bacterial titers were determined. While *ndr1* and the receptor mutant *rps2* showed the expected increased susceptibility to *Pst* DC3000 (AvrRpt2) and the *rpm1* receptor mutant control to *Pst* DC3000 (AvrRpm1) infection, bacterial growth in *swn*, *clf*, and *kyp* mutants did not change significantly in comparison to the wild-type (Figure 7G and H). These results confirm previous evidence that changes in HR cell death are often uncoupled from bacterial growth restriction (Coll et al., 2010; Heidrich et al., 2011; Munch et al., 2015) and suggest that the observed effects are not caused by altered immune receptor expression.

Overall, we conclude that H3K27me3 and H3K9me2 dampen pathogen-induced PCD, revealing a functional role of both epigenetic pathways in controlling the plant pathogen response.

### Discussion

The PRC2 governs the correct execution of developmental programs by epigenetically repressing major regulators of specific developmental transitions (Mozgova and Hennig, 2015). In this study, we employed the inducible expression of two different effectors to unravel the epigenetic changes associated with the pathogen-triggered switch to immunity- and disease-related PCD. We found that effector-induced PCD was associated with substantial changes in the distribution of PRC2-mediated H3K27me3, which was associated with transcriptional changes. PRC2 targets that were transcriptionally upregulated upon PCD induction are related to immune responses and plant senescence, revealing a central role of the PRC2 in repressing effector-triggered PCD in the absence of pathogen infection. Conversely, genes that gained H3K27me3 and became downregulated were enriched for NAC and MADS-box transcription factors, with many of those known to be positive regulators of developmental PCD (Kubo et al., 2005; Zhou et al., 2014; Ohashi-Ito et al., 2018; Tan et al., 2018). Furthermore, we found an ABA response element to be enriched in the promoter region of downregulated genes gaining H3K27me3, indicating that PRC2 is dampening the onset of PCD triggered by pathogen

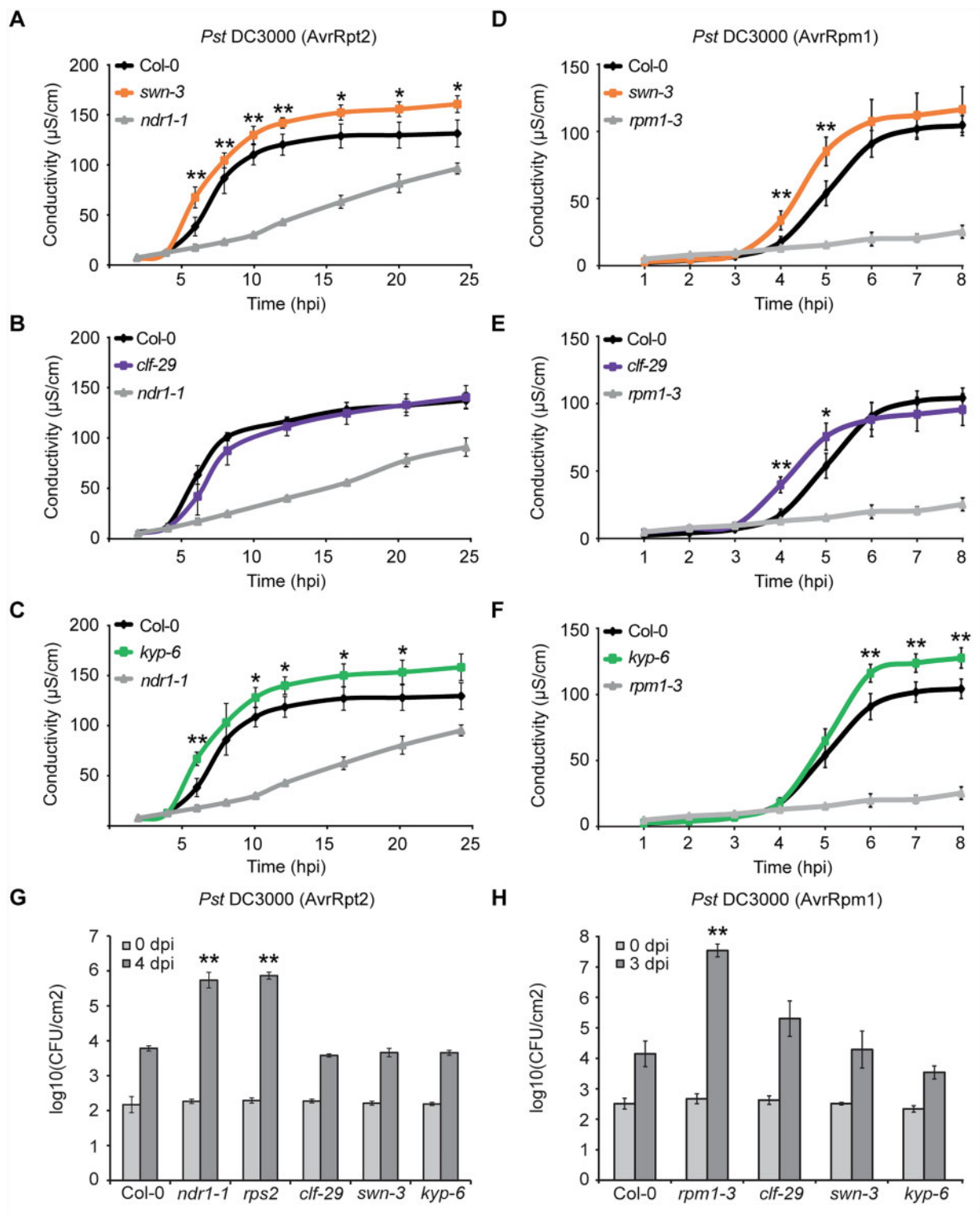


**Figure 7** Effect of loss-of-function mutations in H3K27me3 and H3K9me2 methyltransferases on pathogen-triggered PCD and disease resistance. A–F, Ion leakage in leaves of 5-week-old Col-0 wild-type, *swn-3*, *clf-29*, and *kyp-6* after inoculation with avirulent strains of *Pst* DC3000 harboring AvrRpt2 (A–C) or AvrRpm1 (D–F). *ndr1-1* (A–C) and *rpm1-3* (D–F) mutants served as fully HR-compromised negative controls for proper PCD induction. Mean and SD were calculated from four disks per treatment with four replicates within an experiment. The experiments were repeated at least 3 times and representative data are shown. Statistical significance was tested with a two-tailed t test (\* $P < 0.05$ , \*\* $P < 0.01$ ). Data for (A) and (C) as well as for (D–F) were derived from the same experiments, respectively, but were separated for better legibility. G and H, Growth of avirulent *Pst* DC3000 strains expressing AvrRpt2 (G) or AvrRpm1 (H) in leaves of 5-week-old Col-0 wild-type, *clf-29*, *swn-3*, and *kyp-6* plants 0 and 4 d (G) or 3 d (H) after infiltration at  $OD_{600} = 0.00001$ . *ndr1-1* and *rps2-101c* (G) or *rpm1-3* (H) served as susceptible controls for proper resistance responses. Log-transformed values are means SD with  $n = 4$ . Asterisks indicate statistical significance ( $P < 0.01$ ) determined by one-way ANOVA with post hoc Tukey's test (compared with the wild type).

effectors possibly by blocking the action of ABA. In support of this notion, we found that loss of the PRC2 subunit SWN enhanced progression of PCD, resembling previously reported findings for enhanced ABA-induced PCD in mutants deficient for PRC2 function (Liu et al., 2019). Importantly, it was previously shown that H3K27me3 marked ABA-induced senescence genes remain ABA-responsive (Liu et al., 2019), indicating that the presence of H3K27me3 dampens, but does not block transcription. Similarly, the observation that positive regulators of PCD gain H3K27me3 suggests that the transcription of those genes is attenuated rather than completely blocked. Consistently, PRC2 was proposed to dampen the transcription of a subset of genes in mammalian cells (Young et al., 2011; Kar et al., 2017). Previous work proposed a role for MEDEA, a subunit of the FERTILIZATION INDEPENDENT SEED-PRC2 that is specific for female gametophyte and endosperm development (Roy et al., 2018), in attenuating the response to AvrRpt2. MEDEA was shown to bind and suppress transcription of the immune receptor encoding RPS2 gene (Roy et al., 2018). While indeed MEDEA expression was significantly elevated upon AvrRpt2 and NPP1 induction (Supplemental Data Set S2), expression of RPS2 did not change (Supplemental Data Set S2), questioning whether attenuation of the PRC2-mediated response to AvrRpt2 is mediated via repression of RPS2. This notion is further supported by our observation that RPS2-triggered bacterial growth restriction is unaffected in PRC2 mutants.

Gain and loss of H3K27me3 are achieved by the specific recruitment of PRC2 and H3K27me3 demethylases, respectively (Mozgova and Köhler, 2016). Previous work revealed that the H3K27me3 demethylase REF6 promotes senescence by removing H3K27me3 from SAGs (Wang et al., 2019). While we did not find significant enrichment for REF6 target sites (Cui et al., 2016; Li et al., 2016) among genes losing H3K27me3 upon effector induction, it is possible that recruitment of REF6 or its paralogs EARLY FLOWERING 6 and JUMONJI 13 is mediated by transcription factors that remain to be identified (Yan et al., 2018).

In addition to the redistribution of H3K27me3, we observed decondensation of chromatin during PCD, similar to the previously reported decondensation of chromocenters during *A. thaliana* leaf senescence (Ay et al., 2014). This suggests that PCD is generally associated with global chromatin changes, independent of the triggering event. We found that changes in nuclear architecture were accompanied by a redistribution of H3K9me2 that is likely functionally relevant since the loss of the major H3K9me2 methyltransferase KYP caused increased progression of PCD. Possibly the invasion of H3K9me2 into non-centromeric regions delays PCD by reducing expression of PCD promoting genes, similar to the proposed functional role of PRC2-mediated H3K27me3. Mutants in CROWDED NUCLEI (CRWN) genes form small nuclei with reduced chromocenters (Wang et al., 2013), similar to the phenotype we observed upon PCD induction. Strikingly, deficiencies in CRWN function cause spontaneous

cell death lesions and ectopic induction of defense responses (Choi et al., 2019), supporting the notion that reduced nuclear size and chromocenter decondensation are hallmarks of PCD.

Together, our study reveals that the terminal transition to PCD upon pathogen infection is under tight control by repressive epigenetic pathways that prevent the precocious onset of PCD. This resembles the PRC2-mediated control of senescence, revealing that developmental PCD and pathogen-induced PCD are controlled by similar epigenetic mechanisms, despite triggering a distinct transcriptional response (Chang et al., 2013; Olvera-Carrillo et al., 2015; Liu et al., 2019).

## Materials and methods

### Plant material and growth conditions

All seeds were surface-sterilized using 70% and 90% ethanol (v/v), stratified for 2 d at 4°C, germinated in soil, and grown under short-day conditions (8-h light, 16-h dark) in a growth cabinet at 150  $\mu\text{E m}^{-2} \text{s}^{-1}$ , 21°C, and 70% relative humidity. After 6 weeks, plants were vacuum infiltrated with 2  $\mu\text{M}$  17 $\beta$ -estradiol or mock (ddH<sub>2</sub>O) to induce the expression of transgenes (Brand et al., 2006) and incubated for additional 12 h under continuous light. For bacterial electrolyte leakage and resistance assays, the previously described *ndr1-1* (CS6358; Century et al., 1995), *rps2-101c* (Mindrinos et al., 1994), *rpm1-3* (CS8637; Grant et al., 1995), *swn-3* (SALK\_050195; Chanvivattana et al., 2004), *clf-29* (SALK\_021003; Bouveret et al., 2006), and *kyp-6* (SALK\_041474; Chan et al., 2006) mutants were used.

### Plasmid construction and plant transformation

For the generation of the inducible NPP1 line, the SP of *Daucus carota* *extensin* was amplified by PCR from a SP-PaNie expressing *A. thaliana* line (Rauhut et al., 2009) using the primers 5'-CACCATGGGAAGAATTGCTAGAGGC-3' (fwd), and AAGCTTATGGATCCAGCTGTGGTTTCGGAA GCC (rev). The resulting PCR product with 3'-terminally introduced BamHI/HindIII sites was inserted into pENTR/D-TOPO. NPP1 was amplified from the plasmid pPIC9K-PpNLP (Ottmann et al., 2009) using primers 5'-TTTTG GATCCGACGTGATCTCGCACGATGC-3' (fwd), and 5'-TTTAAAGCTTAGCGTAGTAAGCGTTGCCTAC-3' (rev) and inserted 3'-terminally to the SP in pENTR/D-TOPO between the BamHI and HindIII sites.

For the inducible expression of AvrRpt2, the effector sequence was amplified by PCR from a transgenic *A. thaliana* line (Mackey et al., 2003) using primers 5'-CACCATG AAAATTGCTCCAGTTGCC-fwd) and 5'-GCGGTAGAG CATTGCGTGTGG-3' (rev), and inserted into pENTR/D-TOPO. Both SP-NPP1 and AvrRpt2 were recombined into pGWB614 (Nakagawa et al., 2007) and amplified by PCR to include the 3  $\times$  HA tag using the respective fwd primers and 5'-GGCGCGCCTTAGCTGCACTGAGCAGCGTAATCT-3' (rev). The 3  $\times$  HA tagged gene products were inserted into pENTR/D-TOPO and further recombined into the estradiol-

inducible vector pMDC160 (Brand et al., 2006). Constructs were transformed by *Agrobacterium*-mediated floral dip (Clough and Bent, 1998) into the XVE-driver line (Brand et al., 2006).

### Trypan blue staining

Leaves of 6-week-old plants were vacuum-infiltrated with 2  $\mu$ M 17 $\beta$ -estradiol or ddH<sub>2</sub>O (mock) and incubated for 0, 4, 8, 12, and 24 h under continuous light. Leaves were placed in 50 mL falcon tubes, covered with 0.05% (v/v) trypan blue, and boiled in a water bath for 2–3 min. Samples were left in the staining solution for 12 h, then rinsed once in water and thereafter de-stained in chloral hydrate for 4 d. Stained leaves were mounted in 60% (v/v) glycerol and images were acquired using either a Zeiss AxioScope A1 microscope with a Plan-Neofluar 10 $\times$ /0.30 objective connected to a AxioCam IC camera or a Leica M205 FA stereo microscope with a Plan Apo 0.63 $\times$  objective connected to a DMC 4500 camera.

### RNA extraction and RT-qPCR analyses

RNA was extracted from samples 12 h after induction from three independent biological replicates using TRIzol reagent (Invitrogen, Carlsbad, CA, USA), treated with Turbo DNase (Thermo Fisher Scientific, Waltham, MA, USA). Sequencing libraries were prepared using TruSeq RNA Library Preparation Kit version 2 (Illumina, San Diego, CA, USA) and 18 samples were pooled for sequencing in one lane of the Illumina HiSeq2000 platform. cDNA synthesis was performed from 1  $\mu$ g of total RNA using the RevertAid H Minus First Strand cDNA Synthesis Kit (Thermo Fisher Scientific) with oligo dT primers according to producer's instructions. cDNA was diluted 1:5 and RT-qPCR was performed using 2  $\mu$ L of cDNA per 20  $\mu$ L reaction with the 5 $\times$  HOT FIREPol Eva Green qPCR Mix Plus (ROX) kit (Solis Biodyne, Tartu, Estonia) on a CFX96 Touch Real-Time PCR Detection System (Bio-Rad, Hercules, CA, USA). Fold changes were calculated relative to XVE samples using the standard curve method. qPCR experiments were performed following the MIQE guidelines (Bustin et al., 2009). *PP2A* (AT1G69960) was used as the reference gene. Primers used in this study are listed in Supplemental Table S1.

### ChIPseq

For chromatin immunoprecipitation, leaf material at 12 h after induction was collected in PBS (137 mM NaCl, 2.7 mM KCl, 4.3 mM Na<sub>2</sub>HPO<sub>4</sub>, and 1.4 mM KH<sub>2</sub>PO<sub>4</sub>) supplemented with 0.1% (v/v) Tween-20 and cross-linked using 1% (v/v) formaldehyde for 10 min under vacuum. Cross-linking was stopped by glycine at a final concentration of 125 mM for 5 min under vacuum. Leaves were rinsed with water, blotted dry, and frozen in liquid nitrogen. About 200 mg of liquid nitrogen-frozen leaves were used for crude nuclei extraction for ChIP experiments as previously described (Mozgová et al., 2015) from three independent biological replicates. The antibodies used in this study were as follows: anti-H3K27me3 (07-449; Millipore, Burlington, MA, USA) and

anti-H3K9me2 (pAb-060-050; Diagenode, Liege, Belgium). Each experiment was performed in four biological replicates. Sequencing libraries were prepared with the Microplex Library Preparation kit version 2 (Diagenode) using 2 ng of eluted DNA as starting material and 12 samples were pooled for sequencing in one lane of Illumina HiSeq 2000 platform.

### RNAseq data analysis

Untrimmed reads were mapped to the *A. thaliana* reference genome TAIR10 using STAR version 2.5.3.a (Dobin et al., 2013). Expression counts were generated using the R function summarizeOverlaps from the package HTSeq in union mode on exons from the reference transcriptome AtRTD2 (Zhang et al., 2017). Statistics of read mapping can be found in Supplemental Data Set S1. Pearson correlation coefficients for three biological replicates are shown in Supplemental Figure S8. Differential expression analyses were performed using the R package DESeq2 version 1.20.0 (Love et al., 2014). Genes with absolute log<sub>2</sub>FoldChange  $\geq$  1 and false discovery rate (FDR)  $\leq$  0.05 were considered as differentially expressed. Similarly, differential expression analysis for TEs was performed by mapping untrimmed reads to the indexed FASTA sequences of the 31,189 TAIR10 annotated TEs using bowtie2 version 2.2.9 (Langmead and Salzberg, 2012). The read count matrix along individual TEs was prepared with TEcount.py from the software package TETools version 1.0.0-283c1ca (Lerat et al., 2016) and imported into R to perform differential expression analysis using DESeq2 and the same threshold values as for gene transcripts. GO analyses were performed using web-based tool PLAZA version 4.0 (Van Bel et al., 2018). Statistical significance of enriched GO terms was tested with hypergeometric distribution and the Bonferroni method.

### ChIP-seq data analyses

Single-end, 50 bp reads were generated on a HiSeq2500. Reads were mapped to the TAIR10 reference genome with bowtie (-v 2 -m 1; Langmead et al., 2009). The similarity of the biological replicates was assessed by comparing the pairwise correlation of the enrichment scores along genes and TEs (Supplemental Figure S3). Replicates were merged to increase the genomic coverage and statistical power to detect differentially enriched regions (Supplemental Data Set S1B). ChIP-enriched regions were called with SICER (Zang et al., 2009) using the input as the control library (window size = 200 bp, gap size = 600 bp, FDR = 0.01). Significant differences of enrichment between the PCD-inducible and the mock samples were calculated with SICER-diff (Redundancy threshold = 1, window size = 200 bp, gap size = 600 bp, and FDR = 0.01). H3K27me3 score was determined as average coverage of the normalized epigenetic mark along the annotated coordinates of the gene.

### Analysis of cis-element enrichment

Overrepresentation analysis of hexamers on the promoters of sets of genes was performed as previously described (Maruyama et al., 2012) using the 1-kb upstream regions

from the translational start sites obtained through Phytozome version 12 (<https://phytozome.jgi.doe.gov/pz/portal.html>).

### Cytogenetic analyses

Leaves at 12 h after induction of PCD were fixed in 3:1 ethanol/acetic acid and stored at 4°C. Interphase nuclear spreads for DAPI staining and FISH were prepared as previously described (Fransz et al., 2002). Briefly, leaves were rinsed in citrate buffer (10 mM Na Citrate, pH 4.5) and incubated in an enzyme mix [(0.3% (w/v) pectolyase (Sigma, St. Louis, MO, USA), 0.3% (w/v) cytohelicase (Sepracor, Marlborough, MA, USA), and 0.3% (w/v) cellulase (Sigma)] in citrate buffer for 2 h at 37°C. Digested leaves were softened in 100  $\mu$ L 60% (v/v) acetic acid on a non-coated, ethanol cleaned, microscopic slide, spread at 45°C, fixed with ice-cold ethanol/acetic acid (3:1), and dried. The dried preparations were mounted in Vectashield containing DAPI (Vector Laboratories, Burlingame, CA, USA) and used for nuclear size and chromocenter number measurements. Imaging was performed with a Leica DMI4000 inverted microscope, a Leica DFC360FX camera, and LAS AF (Leica Microsystems, Wetzlar, Germany) software. Statistical significance of differences in nuclear size and number of chromocenters was tested with Wilcoxon statistical test.

### FISH

FISH was performed on dried preparations of nuclei from PCD samples 12 h after induction as described (Simon et al., 2018) using directly labeled Locked Nucleic Acid probes (Exiqon, Vedbæk, Denmark) specific for 180 bp centromeric repeats TEX615\_GTATGATTGAGTATAAGAAGCTAAACCG. Hybridization was performed for 1 h at 50°C. Post-hybridization washes were carried out at 55°C twice in  $2 \times$  SSC and once in  $0.75 \times$  SSC. Slides were mounted in Vectashield containing DAPI (Vector Laboratories). Imaging was performed with a Leica DMI4000 inverted microscope, a Leica DFC360FX camera, and LAS AF (Leica Microsystems) software.

### Immunoblot analysis

Proteins were extracted in 100 mM Tris pH 7.5 with 2% (w/v) SDS, boiled for 5 min in Lämmli sample buffer, and cleared by centrifugation. The protein extracts were then separated by SDS-PAGE, transferred to polyvinylidene difluoride membranes (GE Healthcare, Amersham, UK), blocked with 5% (w/v) skimmed milk in PBS, and incubated with an anti-HA primary antibody (Santa Cruz Biotechnology, Dallas, TX, USA) using 1:1,000 dilution in PBS containing 0.1% (v/v) Tween-20. This was followed by incubation with a secondary horseradish peroxidase-conjugated antibody diluted 1:10,000 in PBS 0.1% (v/v) Tween-20 (GE Healthcare, Amersham, UK). The immunoreaction was developed using the ECL Prime kit (GE Healthcare, Amersham, UK) and detected with a LAS-3000 Luminescent Image Analyzer (Fujifilm, Tokyo, Japan).

### Electrolyte leakage and bacterial resistance assays

For quantification of PCD levels, ion leakage assays following estradiol-induced effector expression or syringe-infiltration of avirulent *Pst* DC3000 strains expressing AvrRpt2 (with  $1 \times 10^8$  colony-forming unit [CFU]  $\text{mL}^{-1}$ ) or AvrRpm1 (with  $5 \times 10^7$  CFU  $\text{mL}^{-1}$ ) were performed as described (Hofius et al., 2009; Üstün et al., 2018). Bacterial growth assays were done in 5-week-old plants upon infection with avirulent *Pst* DC3000 (AvrRpt2) or (AvrRpm1) at  $\text{OD}_{600} = 0.00001$  essentially as described (Mackey et al., 2003). Statistical significance for ion leakage was tested with two-tailed *t* test, for bacterial growth assay with one-way ANOVA with post hoc Tukey's test.

### Accession numbers

Sequencing reads are deposited in Gene Expression Omnibus (GSE140410). Sequence data from this article can be found in the *A. thaliana* Information Resource or GenBank/EMBL databases under the following accession numbers: *NDR1* (AT3G20600), *RPM1* (AT3G07040), *RPS2* (AT4G26090) *SWN* (AT4G02020), *CLF* (AT2G23380), *KYP* (AT5G13960).

### Supplemental data

The following materials are available in the online version of this article.

**Supplemental Figure S1.** Reliability of the two-component vector system for induction of effector-mediated PCD.

**Supplemental Figure S2.** Profiles of the PCD transcriptomes.

**Supplemental Figure S3.** Reproducibility of the ChIP-seq biological replicates.

**Supplemental Figure S4.** IGV screenshots showing the distribution of epigenetic marks in biological replicates.

**Supplemental Figure S5.** Changes in H3K9me2 on TE families.

**Supplemental Figure S6.** Loss of H3K27me3 associated with increased expression of hormone-induced genes upon AvrRpt2- and NPP1-induced PCD.

**Supplemental Figure S7.** Analysis of CLF/SWN PRC2-specific gene suppressive mechanisms upon effector-triggered PCD.

**Supplemental Figure S8.** Reproducibility of the RNA-seq biological replicates.

**Supplemental Table S1.** List of primers used in this study.

**Supplemental Data Set S1.** Read statistics of epigenome and transcriptome data.

**Supplemental Data Set S2.** List of up and downregulated genes.

**Supplemental Data Set S3.** List of up and downregulated TEs.

**Supplemental Data Set S4.** List of genes gaining and losing H3K27me3.

**Supplemental Data Set S5.** Correlation of epigenome and transcriptome data.

**Supplemental Data Set S6.** List of genes losing H3K27me3 that are common with genes deregulated in response to different hormones.

**Supplemental Data Set S7.** List of downregulated genes gaining H3K27me3 upon AvrRpt2-induced PCD.

## Acknowledgments

We wish to thank David Mackey (Ohio State University, Columbus, OH, USA) for providing seeds of the Dex-AvrRpt2 expressing *A. thaliana* line, and Isabell Albert and Thorsten Nürnberger (ZMBF, University of Tübingen, Germany) for the pPIC9K-PpNLP plasmid and Alc:SP-PaNie *A. thaliana* line. We also thank the Uppsala Multidisciplinary Center for Advanced Computational Science for providing computing and storage resources for RNAseq data (project SNIC 2017/7-6).

## Funding

This research was supported by grants from the Knut and Alice Wallenberg Foundation (grant no. 2012.0087 to L.H., C.K., and D.H.) and the Carl Tryggers Foundation (to L.H.). Sequencing was performed by the SNP&SEQ Technology Platform, Science for Life Laboratory at Uppsala University, a national infrastructure supported by the Swedish Research Council and the Knut and Alice Wallenberg Foundation.

*Conflict of interest statement.* None declared.

## References

- Albert I, Böhm H, Albert M, Feiler CE, Imkamp J, Wallmeroth N, Brancato C, Raaymakers TM, Oome S, Zhang H et al. (2015) An RLP23–SOBIR1–BAK1 complex mediates NLP-triggered immunity. *Nat Plants* **1**: 15140
- Ay N, Janack B, Humbeck K (2014) Epigenetic control of plant senescence and linked processes. *J Exp Bot* **65**: 3875–3887
- Balazadeh S, Siddiqui H, Allu AD, Matallana-Ramirez LP, Caldana C, Mehrnia M, Zanon M-I, Köhler B, Mueller-Roeber B (2010) A gene regulatory network controlled by the NAC transcription factor ANAC092/AtNAC2/ORE1 during salt-promoted senescence. *Plant J* **62**: 250–264
- Bari R, Jones JDG (2009) Role of plant hormones in plant defence responses. *Plant Mol Biol* **69**: 473–488
- Bell O, Tiwari VK, Thomä NH, Schübeler D (2011) Determinants and dynamics of genome accessibility. *Nat Rev Genet* **12**: 554–564
- Böhm H, Albert I, Oome S, Raaymakers TM, Van den Ackerveken G, Nürnberger T (2014) A conserved peptide pattern from a widespread microbial virulence factor triggers pattern-induced immunity in *Arabidopsis*. *PLoS Pathog* **10**: e1004491
- Bouchez O, Huard C, Lorrain S, Roby D, Balagué C (2007) Ethylene is one of the key elements for cell death and defense response control in the *Arabidopsis* lesion mimic mutant vad1. *Plant Physiol* **145**: 465–477
- Bouveret R, Schonrock N, Gruissem W, Hennig L (2006) Regulation of flowering time by *Arabidopsis* MSI1. *Development* **133**: 1693–1702
- Brand L, Hörler M, Nüesch E, Vassalli S, Barrell P, Yang W, Jefferson RA, Grossniklaus U, Curtis MD (2006) A versatile and reliable two-component system for tissue-specific gene induction in *Arabidopsis*. *Plant Physiol* **141**: 1194–1204
- Breeze E, Harrison E, McHattie S, Hughes L, Hickman R, Hill C, Kiddle S, Kim Y, Penfold CA, Jenkins D et al. (2011) High-resolution temporal profiling of transcripts during *Arabidopsis* leaf senescence reveals a distinct chronology of processes and regulation. *Plant Cell* **23**: 873–894
- Bustin SA, Benes V, Garson JA, Hellemans J, Huggett J, Kubista M, Mueller R, Nolan T, Pfaffl MW, Shipley GL et al. (2009) The MIQE guidelines: minimum information for publication of quantitative real-time PCR experiments. *Clin Chem* **55**: 611–622
- Century KS, Holub EB, Staskawicz BJ (1995) NDR1, a locus of *Arabidopsis thaliana* that is required for disease resistance to both a bacterial and a fungal pathogen. *Proc Natl Acad Sci USA* **92**: 6597–601
- Chan SWL, Henderson IR, Zhang X, Shah G, Chien JSC, Jacobsen SE (2006) RNAi, DRD1, and histone methylation actively target developmentally important non-CG DNA methylation in *Arabidopsis*. *PLoS Genet* **2**: e83
- Chang KN, Zhong S, Weirauch MT, Hon G, Pelizzola M, Li H, Carol Huang SS, Schmitz RJ, Ulrich MA, Kuo D et al. (2013) Temporal transcriptional response to ethylene gas drives growth hormone cross-regulation in *Arabidopsis*. *eLife* **2013**: 1–20
- Chanvivattana Y, Bishopp A, Schubert D, Stock C, Moon YH, Sung ZR, Goodrich J (2004) Interaction of Polycomb-group proteins controlling flowering in *Arabidopsis*. *Development* **131**: 5263–5276
- Choi J, Strickler SR, Richards EJ (2019) Loss of CRWN nuclear proteins induces cell death and salicylic acid defense signaling. *Plant Physiol* **179**: 1315–1329
- Clough SJ, Bent A F (1998) Floral dip: a simplified method for *Agrobacterium*-mediated transformation of *Arabidopsis thaliana*. *Plant J* **16**: 735–743
- Coll NS, Epple P, Dangl JL (2011) Programmed cell death in the plant immune system. *Cell Death Differ* **18**: 1247–1256
- Coll NS, Vercammen D, Smidler A, Clover C, Van Breusegem F, Dangl JL, Epple P (2010) *Arabidopsis* type I metacaspases control cell death. *Science* **330**: 1393–1397
- Cui X, Lu F, Qiu Q, Zhou B, Gu L, Zhang S, Kang Y, Cui X, Ma X, Yao Q et al. (2016) REF6 recognizes a specific DNA sequence to demethylate H3K27me3 and regulate organ boundary formation in *Arabidopsis*. *Nat Genet* **48**: 694–699
- Dickman MB, Fluhr R (2013) Centrality of host cell death in plant-microbe interactions. *Annu Rev Phytopathol* **51**: 543–570
- Dobin A, Davis CA, Schlesinger F, Drenkow J, Zaleski C, Jha S, Batut P, Chaisson M, Gingeras TR (2013) STAR: ultrafast universal RNA-seq aligner. *Bioinformatics* **29**: 15–21
- Dong J, Sun N, Yang J, Deng Z, Lan J, Qin G, He H, Deng XW, Irish VF, Chen H et al. (2019) The transcription factors tcp4 and pif3 antagonistically regulate organ-specific light induction of saur genes to modulate cotyledon opening during de-etiolation in *Arabidopsis*. *Plant Cell* **31**: 1155–1170
- Dowen RH, Pelizzola M, Schmitz RJ, Lister R, Dowen JM, Nery JR, Dixon JE, Ecker JR (2012) Widespread dynamic DNA methylation in response to biotic stress. *Proc Natl Acad Sci* **109**: 2183–2191
- Dutta A, Choudhary P, Caruana J, Raina R (2017) JM27, an *Arabidopsis* H3K9 histone demethylase, modulates defense against *Pseudomonas syringae* and flowering time. *Plant J* **91**: 1015–1028
- Ebbs ML, Bender J (2006) Locus-specific control of DNA methylation by the *Arabidopsis* SUVH5 histone methyltransferase. *Plant Cell* **18**: 1166–1176
- Elmore JM, Liu J, Smith B, Phinney B, Coaker G (2012) Quantitative proteomics reveals dynamic changes in the plasma membrane during *Arabidopsis* immune signaling. *Mol Cell Proteomics* **11**: M111.014555
- Fellbrich G, Romanski A, Varet A, Blume B, Brunner F, Engelhardt S, Felix G, Kemmerling B, Krzymowska M, Nürnberger T (2002) NPP1, a Phytophthora-associated trigger of plant defense in parsley and *Arabidopsis*. *Plant J* **32**: 375–390
- Fransz P, de Jong JH, Lysak M, Castiglione MR, Schubert I (2002) Interphase chromosomes in *Arabidopsis* are organized as well

- defined chromocenters from which euchromatin loops emanate. *Proc Natl Acad Sci* **99**: 14584–14589
- Grant MR, Godiard L, Straube E, Ashfield T, Lewald J, Sattler A, Innes RW, Dangl JL** (1995) Structure of the Arabidopsis RPM1 gene enabling dual specificity disease resistance. *Science* **269**: 843–846
- Guo Y, Gan SS** (2012) Convergence and divergence in gene expression profiles induced by leaf senescence and 27 senescence-promoting hormonal, pathological and environmental stress treatments. *Plant Cell Environ* **35**: 644–655
- Hatsugai N, Iwasaki S, Tamura K, Kondo M, Fuji K, Ogasawara K, Nishimura M, Hara-Nishimura I** (2009) A novel membrane fusion-mediated plant immunity against bacterial pathogens. *Genes Dev* **23**: 2496–2506
- Hecker A, Brand LH, Peter S, Simoncello N, Kilian J, Harter K, Gaudin V, Wanke D** (2015) The Arabidopsis GAGA-binding factor BASIC PENTACYSTEINE6 recruits the POLYCOMB-REPRESSIVE COMPLEX1 component LIKE HETEROCHROMATIN PROTEIN1 to GAGA DNA motifs. *Plant Physiol* **168**: 130–141
- Heidrich K, Wirthmueller L, Tasset C, Pouzet C, Deslandes L, Parker JE** (2011) Arabidopsis EDS1 connects pathogen effector recognition to cell compartment-specific immune responses. *Science* **334**: 1401–1404
- Hickman R, Van Verk MC, Van Dijken AJH, Mendes MP, Vroegop-Vos IA, Caarls L, Steenbergen M, Van der Nagel I, Wesselink GJ, Jironkin A et al.** (2017) Architecture and dynamics of the jasmonic acid gene regulatory network. *Plant Cell* **29**: 2086–2105
- Hofius D, Schultz-Larsen T, Joensen J, Tsitsigiannis DI, Petersen NHT, Mattsson O, Jørgensen LB, Jones JDG, Mundy J, Petersen M** (2009) Autophagic Components Contribute to Hypersensitive Cell Death in Arabidopsis. *Cell* **137**: 773–783
- Howard BE, Hu Q, Babaoglu AC, Chandra M, Borghi M, Tan X, He L, Winter-Sederoff H, Gassmann W, Veronese P et al.** (2013) High-throughput RNA sequencing of pseudomonas-infected Arabidopsis reveals hidden transcriptome complexity and novel splice variants. *PLoS One* **8**: e74183
- Huysmans M, Lema A S, Coll NS, Nowack MK** (2017) Dying two deaths — programmed cell death regulation in development and disease. *Curr Opin Plant Biol* **35**: 37–44
- Hwang S, Rhee SY, Marcotte EM, Lee I** (2011) Systematic prediction of gene function in *Arabidopsis thaliana* using a probabilistic functional gene network. *Nat Protoc* **6**: 1429–1442
- Iqbal N, Khan NA, Ferrante A, Trivellini A, Francini A, Khan MIR** (2017) Ethylene role in plant growth, development and senescence: interaction with other phytohormones. *Front Plant Sci* **8**: 1–19
- Jackson JP, Lindroth AM, Cao X, Jacobsen SE** (2002) Control of CpNpG DNA methylation by the KRYPTONITE histone H3 methyltransferase. *Nature* **416**: 556–560
- Jasinski S, Piazza P, Craft J, Hay A, Woolley L, Rieu I, Phillips A, Hedden P, Tsiantis M** (2005) KNOX action in Arabidopsis is mediated by coordinate regulation of cytokinin and gibberellin activities. *Curr Biol* **15**: 1560–1565
- Jin H, Choi SM, Kang MJ, Yun SH, Kwon DJ, Noh YS, Noh B** (2018) Salicylic acid-induced transcriptional reprogramming by the HAC-NPR1-TGA histone acetyltransferase complex in Arabidopsis. *Nucleic Acids Res* **46**: 11712–11725
- Kar G, Kim JK, Kolodziejczyk AA, Natarajan KN, Torlai Triglia E, Mifsud B, Elderkin S, Marioni JC, Pombo A, Teichmann SA** (2017) Flipping between Polycomb repressed and active transcriptional states introduces noise in gene expression. *Nat Commun* **8**: 36
- Kassia JA, Brown JL** (2013) Polycomb group response elements in drosophila and vertebrates. *Adv Genet* **81**: 83–118
- Kim HJ, Park JH, Kim J, Kim JJ, Hong S, Kim J, Kim JH, Woo HR, Hyeon C, Lim PO et al.** (2018) Time-evolving genetic networks reveal a nac troika that negatively regulates leaf senescence in arabidopsis. *Proc Natl Acad Sci USA* **115**: E4930–E4939
- Kim J, Chang C, Tucker ML** (2015) To grow old: regulatory role of ethylene and jasmonic acid in senescence. *Front Plant Sci* **6**: 1–7
- Koussevitsky S, Nott A, Mockler TC, Hong F, Sachetto-Martins G, Surpin M, Lim J, Mittler R, Chory J** (2007) Signals from chloroplasts converge to regulate nuclear gene expression. *Science* **316**: 715–719
- Kubo M, Udagawa M, Nishikubo N, Horiguchi G, Yamaguchi M, Ito J, Mimura T, Fukuda H, Demura T** (2005) Transcription switches for protoxylem and metaxylem vessel formation. *Genes Dev* **19**: 1855–1860
- Lai Z, Mengiste T** (2013) Genetic and cellular mechanisms regulating plant responses to necrotrophic pathogens. *Curr Opin Plant Biol* **16**: 505–512
- Langmead B, Salzberg SL** (2012) Fast gapped-read alignment with Bowtie 2. *Nat Methods* **9**: 357–359
- Langmead B, Trapnell C, Pop M, Salzberg SL** (2009) Ultrafast and memory-efficient alignment of short DNA sequences to the human genome. *Genome Biol* **10**: R25
- Lenarčić T, Albert I, Böhm H, Hodnik V, Pirc K, Zavec AB, Podobnik M, Pahovnik D, Žagar E, Pruitt R et al.** (2017) Eudicot plant-specific sphingolipids determine host selectivity of microbial NLP cytolytins. *Science* **358**: 1431–1434
- Lerat E, Fablet M, Modolo L, Lopez-Maestre H, Vieira C** (2016) TTools facilitates big data expression analysis of transposable elements and reveals an antagonism between their activity and that of piRNA genes. *Nucleic Acids Res* **45**: e17
- Li C, Gu L, Gao L, Chen C, Wei CQ, Qiu Q, Chien CW, Wang S, Jiang L, Ai LF et al.** (2016) Concerted genomic targeting of H3K27 demethylase REF6 and chromatin-remodeling ATPase BRM in Arabidopsis. *Nat Genet* **48**: 687–693
- Lim G-H, Singhal R, Kachroo A, Kachroo P** (2017) Fatty acid- and lipid-mediated signaling in plant defense. *Annu Rev Phytopathol* **55**: 505–536
- Lim MTS, Kunkel BN** (2004) The *Pseudomonas syringae* type III effector AvrRpt2 promotes virulence independently of RIN4, a predicted virulence target in *Arabidopsis thaliana*. *Plant J* **40**: 790–798
- Liu C, Chen H, Er HL, Soo HM, Kumar PP, Han JH, Liou YC, Yu H** (2008) Direct interaction of AGL24 and SOC1 integrates flowering signals in Arabidopsis. *Development* **135**: 1481–1491
- Liu C, Cheng J, Zhuang Y, Ye L, Li Z, Wang Y, Qi M, Xu L, Zhang Y** (2019) Polycomb repressive complex 2 attenuates ABA-induced senescence in Arabidopsis. *Plant J* **97**: 368–377
- López Sánchez A, Stassen JHM, Furci L, Smith LM, Ton J** (2016) The role of DNA (de)methylation in immune responsiveness of Arabidopsis. *Plant J* **88**: 361–374
- Love MI, Huber W, Anders S** (2014) Moderated estimation of fold change and dispersion for RNA-seq data with DESeq2. *Genome Biol* **15**: 550
- Mackey D, Belkhadir Y, Alonso JM, Ecker JR, Dangl JL** (2003) Arabidopsis RIN4 is a target of the type III virulence effector AvrRpt2 and modulates RPS2-mediated resistance. *Cell* **112**: 379–389
- Maruyama K, Todaka D, Mizoi J, Yoshida T, Kidokoro S, Matsukura S, Takasaki H, Sakurai T, Yamamoto YY, Yoshiwara K et al.** (2012) Identification of cis-acting promoter elements in cold- and dehydration-induced transcriptional pathways in arabidopsis, rice, and soybean. *DNA Res* **19**: 37–49
- McNellis TW, Mudgett MB, Li K, Aoyama T, Horvath D, Chua NH, Staskawicz BJ** (1998) Glucocorticoid-inducible expression of a bacterial avirulence gene in transgenic Arabidopsis induces hypersensitive cell death. *Plant J* **14**: 247–57
- Mindrin M, Katagiri F, Yu GL, Ausubel FM** (1994) The *A. thaliana* disease resistance gene RPS2 encodes a protein containing a nucleotide-binding site and leucine-rich repeats. *Cell* **78**: 1089–1099
- Montillet JL, Chamnongpol S, Rustérucci C, Dat J, van de Cotte B, Agnel JP, Battesti C, Inzé D, Van Breusegem F, Triantaphyllidis C** (2005) Fatty acid hydroperoxides and H<sub>2</sub>O<sub>2</sub> in the execution

- of hypersensitive cell death in tobacco leaves. *Plant Physiol* **138**: 1516–1526
- Moreno-Romero J, Jiang H, Santos-González J, Köhler C** (2016) Parental epigenetic asymmetry of PRC 2-mediated histone modifications in the Arabidopsis endosperm. *EMBO J* **35**: 1298–1311
- Mozgova I, Hennig L** (2015) The polycomb group protein regulatory network. *Annu Rev Plant Biol* **66**: 269–296
- Mozgova I, Köhler C** (2016) DNA-sequence-specific erasers of epigenetic memory. *Nat Genet* **48**: 591–592
- Mozgová I, Wildhaber T, Liu Q, Abou-Mansour E, L'Haridon F, Métraux JP, Grisse W, Hofius D, Hennig L** (2015) Chromatin assembly factor CAF-1 represses priming of plant defence response genes. *Nat Plants* **1**: 15127
- Mukhtar MS, McCormack ME, Argueso CT, Pajeroska-Mukhtar KM** (2016) Pathogen tactics to manipulate plant cell death. *Curr Biol* **26**: 608–619
- Munch D, Teh OK, Malinovsky FG, Liu Q, Vetukuri RR, El Kasmi F, Brodersen P, Hara-Nishimura I, Dangl JL, Petersen M et al.** (2015) Retromer contributes to immunity-associated cell death in Arabidopsis. *Plant Cell* **27**: 463–479
- Nakagawa T, Kurose T, Hino T, Tanaka K, Kawamukai M, Niwa Y, Toyooka K, Matsuoka K, Jinbo T, Kimura T** (2007) Development of series of gateway binary vectors, pGWBs, for realizing efficient construction of fusion genes for plant transformation. *J Biosci Bioeng* **104**: 34–41
- Ohashi-Ito K, Iwamoto K, Fukuda H** (2018) LOB DOMAIN-CONTAINING PROTEIN 15 positively regulates expression of VND7, a master regulator of tracheary elements. *Plant Cell Physiol* **59**: 989–996
- Olvera-Carrillo Y, Van Bel M, Van Hautegeem T, Fendrych M, Van Durme M, Huysmans M, Šimášková M, Buscaill P, Rivas S, Coll NS et al.** (2015) A conserved core of PCD indicator genes discriminates developmentally and environmentally induced programmed cell death in plants. *Plant Physiol* **169**: 00769
- Ottmann C, Luberacki B, Kufner I, Koch W, Brunner F, Weyand M, Mattinen L, Pirhonen M, Anderluh G, Seitz HU et al.** (2009) A common toxin fold mediates microbial attack and plant defense. *Proc Natl Acad Sci* **106**: 10359–10364
- Podzimská-Sroka D, O'Shea C, Gregersen PL, Skriver K** (2015) NAC transcription factors in senescence: from molecular structure to function in crops. *Plants* **4**: 412–448
- Qutob D, Kemmerling B, Brunner F, Kufner I, Engelhardt S, Gust AA, Luberacki B, Seitz HU, Stahl D, Rauhut T et al.** (2006) Phytotoxicity and innate immune responses induced by Nep1-like proteins. *Plant Cell* **18**: 3721–3744
- Radojčić A, Li X, Zhang Y** (2018) Salicylic acid: a double-edged sword for programmed cell death in plants. *Front Plant Sci* **9**: 1133
- Rauhut T, Luberacki B, Seitz HU, Glawischig E** (2009) Inducible expression of a Nep1-like protein serves as a model trigger system of camalexin biosynthesis. *Phytochemistry* **70**: 185–189
- Le Roux C, Del Prete S, Boutet-Mercey S, Perreau F, Balagué C, Roby D, Fagard M, Gaudin V** (2014) The hnRNP-Q protein LIF2 participates in the plant immune response. *PLoS One* **9**: e99343
- Roy S, Gupta P, Rajabhoj MP, Maruthachalam R, Nandi AK** (2018) The polycomb-group repressor MEDEA attenuates pathogen defense. *Plant Physiol* **177**: 1728–1742
- Safavi-Rizi V, Franzaring J, Fangmeier A, Kunze R** (2018) Divergent N deficiency-dependent senescence and transcriptome response in developmentally old and young Brassica napus leaves. *Front Plant Sci* **9**: 48
- Sato H, Takasaki H, Takahashi F, Suzuki T, Iuchi S, Mitsuda N, Ohme-Takagi M, Ikeda M, Seo M, Yamaguchi-Shinozaki K et al.** (2018) Arabidopsis thaliana NGATHA1 transcription factor induces ABA biosynthesis by activating NCE3 gene during dehydration stress. *Proc Natl Acad Sci USA* **115**: E11178–E11187
- Schultz-Larsen T, Lenk A, Kalinowska K, Vestergaard LK, Pedersen C, Isono E, Thordal-Christensen H** (2018) The AMSH3 ESCRT-III-associated deubiquitinase is essential for plant immunity. *Cell Rep* **25**: 2329–2338
- Shu J, Chen C, Thapa RK, Bian S, Nguyen V, Yu K, Yuan ZC, Liu J, Kohalmi SE, Li C et al.** (2019) Genome-wide occupancy of histone H3K27 methyltransferases CURLY LEAF and SWINGER in Arabidopsis seedlings. *Plant Direct* **3**: e00100 doi: 10.1002/pld3.100
- Simon L, Rabanal FA, Dubos T, Oliver C, Lauber D, Poulet A, Vogt A, Mandlbauer A, Le Goff S, Sommer A et al.** (2018) Genetic and epigenetic variation in 5S ribosomal RNA genes reveals genome dynamics in Arabidopsis thaliana. *Nucleic Acids Res* **46**: 3019–3033
- Tan TT, Endo H, Sano R, Kurata T, Yamaguchi M, Ohtani M, Demura T** (2018) Transcription factors VND1-VND3 contribute to cotyledon xylem vessel formation. *Plant Physiol* **176**: 773–789
- Thaler JS, Humphrey PT, Whiteman NK** (2012) Evolution of jasmonate and salicylate signal crosstalk. *Trends Plant Sci* **17**: 260–270
- Thomas H** (2013) Senescence, ageing and death of the whole plant. *New Phytol* **197**: 696–711
- Trigueros M, Navarrete-Gómez M, Sato S, Christensen SK, Pelaz S, Weigel D, Yanofsky MF, Ferrándiz C** (2009) The NGATHA genes direct style development in the Arabidopsis gynoecium. *Plant Cell* **21**: 1394–1409
- Üstün S, Hafren A, Liu Q, Marshall RS, Minina EA, Bozhkov P V, Vierstra RD, Hofius D** (2018) Bacteria exploit autophagy for proteasome degradation and enhanced virulence in plants. *Plant Cell* **30**: 668–685
- Van Bel M, Diels T, Vancaester E, Kreft L, Botzki A, Van de Peer Y, Coppens F, Vandepoele K** (2018) PLAZA 4.0: an integrative resource for functional, evolutionary and comparative plant genomics. *Nucleic Acids Res* **46**: D1190–D1196
- Wang H, Dittmer TA, Richards EJ** (2013) Arabidopsis CROWDED NUCLEI (CRWN) proteins are required for nuclear size control and heterochromatin organization. *BMC Plant Biol* **13**: 200
- Wang J, Xia H, Zhao SZ, Hou L, Zhao CZ, Ma C Le, Wang XJ, Li PC** (2018) A role of GUNs-Involved retrograde signaling in regulating Acetyl-CoA carboxylase 2 in Arabidopsis. *Biochem Biophys Res Commun* **505**: 712–719
- Wang X, Gao J, Gao S, Song Y, Yang Z, Kuai B** (2019) The H3K27me3 demethylase REF6 promotes leaf senescence through directly activating major senescence regulatory and functional genes in Arabidopsis. *PLoS Genet* **15**: e1008068
- Xiao J, Jin R, Yu X, Shen M, Wagner JD, Pai A, Song C, Zhuang M, Klasfeld S, He C et al.** (2017) Cis and trans determinants of epigenetic silencing by Polycomb repressive complex 2 in Arabidopsis. *Nat Genet* **49**: 1546–1552
- Xu W, Fiume E, Coen O, Pechoux C, Lepiniec L, Magnani E** (2016) Endosperm and nucellus develop antagonistically in Arabidopsis seeds. *Plant Cell* **28**: 1343–1360
- Yan W, Chen D, Smaczniak C, Engelhorn J, Liu H, Yang W, Graf A, Carles CC, Zhou DX, Kaufmann K** (2018) Dynamic and spatial restriction of Polycomb activity by plant histone demethylases. *Nat Plants* **4**: 681–689
- Yolcu S, Li X, Li S, Kim YJ** (2018) Beyond the genetic code in leaf senescence. *J Exp Bot* **69**: 801–810
- Young MD, Willson TA, Wakefield MJ, Tronson E, Hilton DJ, Blewitt ME, Oshlack A, Majewski IJ** (2011) ChIP-seq analysis reveals distinct H3K27me3 profiles that correlate with transcriptional activity. *Nucleic Acids Res* **39**: 7415–7427
- Yu JR, Lee CH, Oksuz O, Stafford JM, Reinberg D** (2019) PRC2 is high maintenance. *Genes Dev* **33**: 903–935
- Zang C, Schones DE, Zeng C, Cui K, Zhao K, Peng W** (2009) A clustering approach for identification of enriched domains from histone modification ChIP-Seq data. *Bioinformatics* **25**: 1952–1958
- Zhang R, Calixto CPG, Marquez Y, Venhuizen P, Tzioutziou NA, Guo W, Spensley M, Entizne JC, Lewandowska D, ten Have S et al.** (2017) A high quality Arabidopsis transcriptome for accurate transcript-level analysis of alternative splicing. *Nucleic Acids Res* **45**: 5061–5073

- Zhang Y, Mayba O, Pfeiffer A, Shi H, Tepperman JM, Speed TP, Quail PH** (2013) A quartet of PIF bHLH factors provides a transcriptionally centered signaling hub that regulates seedling morphogenesis through differential expression-patterning of shared target genes in Arabidopsis. *PLoS Genet* **9**: 1003244
- Zhou J, Wang X, He K, Charron J-BF, Elling AA, Deng XW** (2010) Genome-wide profiling of histone H3 lysine 9 acetylation and dimethylation in Arabidopsis reveals correlation between multiple histone marks and gene expression. *Plant Mol Biol* **72**: 585–595
- Zhou J, Zhong R, Ye ZH** (2014) Arabidopsis NAC domain proteins, VND1 to VND5, are transcriptional regulators of secondary wall biosynthesis in vessels. *PLoS One* **9**: e105726
- Zoeller M, Stingl N, Krischke M, Fekete A, Waller F, Berger S, Mueller MJ** (2012) Lipid profiling of the Arabidopsis hypersensitive response reveals specific lipid peroxidation and fragmentation processes: biogenesis of pimelic and azelaic acid. *Plant Physiol* **160**: 365–378
- Zuo J, Niu QW, Chua NH** (2000) An estrogen receptor-based transactivator XVE mediates highly inducible gene expression in transgenic plants. *Plant J* **24**: 265–273